JEM Journal of Experimental Medicine

BRIEF DEFINITIVE REPORT

ATP spreads inflammation to other limbs through crosstalk between sensory neurons and interneurons

Rie Hasebe[1,2*], Kaoru Murakami[1*], Masaya Harada[4*], Nada Halaka[1*], Hiroshi Nakagawa[5], Fuminori Kawano[6], Yoshinobu Ohira[6], Tadafumi Kawamoto[7], Fiona E. Yull[8], Timothy S. Blackwell[9], Junko Nio-Kobayashi[10], Toshihiko Iwanaga[10], Masahiko Watanabe[11], Nobuhiro Watanabe[12], Harumi Hotta[12], Toshihide Yamashita[5], Daisuke Kamimura[1], Yuki Tanaka[1,3*], and Masaaki Murakami[1,2,3]

Neural circuits between lesions are one mechanism through which local inflammation spreads to remote positions. Here, we show the inflammatory signal on one side of the joint is spread to the other side via sensory neuron–interneuron crosstalk, with ATP at the core. Surgical ablation or pharmacological inhibition of this neural pathway prevented inflammation development on the other side. Mechanistic analysis showed that ATP serves as both a neurotransmitter and an inflammation enhancer, thus acting as an intermediary between the local inflammation and neural pathway that induces inflammation on the other side. These results suggest blockade of this neural pathway, which is named the remote inflammation gateway reflex, may have therapeutic value for inflammatory diseases, particularly those, such as rheumatoid arthritis, in which inflammation spreads to remote positions.

Introduction

One criterion for the fundamental characteristic of rheumatoid arthritis (RA) is remote inflammation, which results in severe malformation and immobility in both sides of the joints (Arnett et al., 1988; Clarke et al., 1994). Similar symptoms are observed in other diseases, including psoriasis and pulmonary fibrosis, and it is reported that a neural mechanism is involved (Kelly et al., 2007; Kidd et al., 1989). However, details about the mechanism have not been demonstrated.

The IL-6 amplifier is a mechanism for tissue-specific inflammation and enhanced NF-κB activation in non-immune cells, including synovial fibroblasts and endothelial cells. Induction of the IL-6 amplifier causes the expression of inflammation mediators including chemokines and growth factors in animal models and RA patients (Murakami et al., 2011; Ogura et al., 2008). In this system, hyperactivation of the NF-κB signal is induced by the simultaneous stimulation of NF-κB and STAT3, followed by local inflammation (Atsumi et al., 2014; Harada et al., 2015; Lee et al., 2013; Murakami et al., 2013; Murakami et al., 2011; Ogura et al., 2008; Okuyama et al., 2018). Since one NF-κB target, IL-6, is the main STAT3 stimulator during inflammation, its paracrine action maintains STAT3 activation to express inflammatory mediators via the IL-6 amplifier in inflammatory diseases (Murakami et al., 2019). Indeed, the IL-6 amplifier plays a role in inflammatory diseases in many organs including the skin, kidney, central nervous system, and lungs (Arima et al., 2012; Fujita et al., 2019; Higuchi et al., 2020; Hirano and Murakami, 2020; Lee et al., 2013; Stofkova et al., 2019; Takada et al., 2020). Accordingly, we have defined inflammation as an IL-6–mediated accumulation of immune cells and/or proliferation of regional non-immune cells, followed by the dysregulation of local homeostasis (Murakami et al., 2019).

In endothelial cells, the IL-6 amplifier is enhanced by sympathetic activation, followed by the establishment of gateways for autoreactive CD4+ T cells to pass blood barriers, a mechanism known as the gateway reflex (Kamimura et al., 2020; Matsuyama et al., 2021). Noradrenaline, which is derived from

[1]Division of Molecular Psychoimmunology, Institute for Genetic Medicine, Graduate School of Medicine, Hokkaido University, Sapporo, Japan; [2]Division of Molecular Neuroimmunology, Department of Homeostatic Regulation, National Institute for Physiological Sciences, National Institutes of Natural Sciences, Aichi, Japan; [3]Group of Quantumimmunology, Institute for Quantum Life Science, National Institute for Quantum and Radiological Science and Technology, Chiba, Japan; [4]Laboratory of Developmental Immunology, Graduate School of Frontier Biosciences, Graduate School of Medicine, and World Premier International Immunology Frontier Research Center, Osaka University, Osaka, Japan; [5]Department of Molecular Neurosciences, Graduate School of Frontier Biosciences, Graduate School of Medicine, and World Premier International Immunology Frontier Research Center, Osaka University, Osaka, Japan; [6]Department of Health and Sports Sciences, Graduate School of Medicine, and Graduate School of Frontier Biosciences, Osaka University, Osaka, Japan; [7]Radioisotope Research Institute, Department of Dental Medicine, Tsurumi University, Yokohama, Japan; [8]Department of Pharmacology, Vanderbilt University, Nashville, TN; [9]Department of Medicine, Vanderbilt University, Nashville, TN; [10]Laboratory of Histology and Cytology, Graduate School of Medicine, Hokkaido University, Sapporo, Japan; [11]Department of Anatomy, Graduate School of Medicine, Hokkaido University, Sapporo, Japan; [12]Department of Autonomic Neuroscience, Tokyo Metropolitan Institute of Gerontology, Tokyo, Japan.

*R. Hasebe, K. Murakami, M. Harada, N. Halaka, and Y. Tanaka contributed equally to this paper. Correspondence to Masaaki Murakami: murakami@igm.hokudai.ac.jp.

sympathetic activation, induces NF-κB activation in local endothelial cells via the amplifier. In gateway reflexes, sympathetic activation is triggered by sensory activation via environmental stimuli and distributed at specific blood vessels to induce gateways for autoreactive T cells, resulting in tissue-specific autoimmune diseases (Arima et al., 2012; Arima et al., 2015; Arima et al., 2017; Stofkova et al., 2019). We hypothesized that a similar neural reflex linking inflammation between two sites is involved in the development of spreading inflammation. Further, since several neurotransmitters activate or suppress NF-κB and/or STAT3 pathways (Murase and McKay, 2014; Nicolas et al., 2012) and because we showed that ATP induced by brain microinflammation activates new neural pathways followed by inflammation of remote organs with sudden death (Arima et al., 2017), we considered whether the secretion of neurotransmitters causes the inflammation to spread.

The gateway reflex is just one mechanism regulating crosstalk between the nervous and immune systems. For example, after chemical sympathectomy, the severity of experimental autoimmune encephalomyelitis worsens (Chelmicka-Schorr et al., 1992), suggesting that the sympathetic nervous system exerts a regulatory effect on the immune response. Moreover, Molleston et al. (1993) showed that optic nerve transections activate microglia in the superior colliculus and localization of the inflammatory lesions on the side of the optic nerve transection. Pavlov and Tracey (2017) showed that vagus nerve stimulation suppressed systemic inflammation in septic models and patients suffering from RA and inflammatory bowel disease as the inflammatory reflex.

F759 mice are a spontaneous RA model dependent on the IL-6 amplifier in the joints (Atsumi et al., 2002; Murakami et al., 2011; Ogura et al., 2008). These mice have an amino acid substitution, Y759F, in gp130, the IL-6 signal transducer in the IL-6R complex (Murakami et al., 2019). Since phosphorylated Y759 is the binding site of SOCS3 for the negative regulation of IL-6 signaling, IL-6–mediated STAT3 activation is enhanced followed by the development of an RA-like disease in both sides of the ankle joints with age. Moreover, an enhanced IL-6 signal in type 1 collagen+ (Col1a+) non-immune cells is responsible for the development of F759 arthritis. Importantly, F759 arthritis was developed even in RAG-deficient F759 mice (Sawa et al., 2006), although F759 arthritis is dependent on Th17 cells expressing IL-17A and IL-6 in a non-RAG-deficient background followed by activation of the IL-6 amplifier in joints by these cytokines (Murakami et al., 2011). In fact, ankle-joint injections of these cytokines in young F759 mice caused an arthritic disease within 2 wk (Harada et al., 2015; Meng et al., 2016; Murakami et al., 2013).

Here, we investigated the molecular mechanism of spreading inflammation as a representative cytokine-induced arthritis model as well as in a collagen-induced arthritis (CIA) model. We show that regional neural interactions between both ankle joints play a critical role in inducing the spread of inflammation via the bilateral expressions of ATP, which activates the neural pathway and enhances inflammation development via the IL-6 amplifier. Our findings suggest that blockade of this neural pathway is a possible therapeutic strategy for various spreading inflammation including arthritis.

Results and discussion

Sensory neurons are critical for spreading inflammation between joints

We previously established cytokine-induced and non-immune cell-triggered arthritis in F759 mice by ankle-joint injections of IL-17A and IL-6 (Atsumi et al., 2017; Murakami et al., 2011; Ota et al., 2020). Histological analysis showed that the synovial cavity is narrowed by hypertrophic synovial fibroblasts and that immune cells, including MHC class II (MHC II)+ and CD4+ cells, accumulate in the affected joint (Murakami et al., 2011; Fig. S1, A and B).

Inflammation can be induced both uni- and bilaterally in this model, which enables us to investigate spreading inflammation from one ankle joint to the other. Inflammation in each joint can be induced when cytokines are injected into either ankle joint (data not shown). Because we hypothesized that spreading inflammation might depend on neural pathways, we performed deafferentation of the sensory neurons at one side of the dorsal root ganglions (DRGs) beside the fifth lumbar cord (L5) to investigate whether the sensory pathway is involved in the development of arthritis in the ankle joints. We injected IL-17A and IL-6 into both ankle joints of F759 mice. The deafferentation of sensory neurons at one side of the L5 DRG reduced the development of arthritis in both ankles (Fig. 1, A and B). We then investigated whether inflammation on one side triggers the development of inflammation on the other side. We injected cytokines into the left ankle and investigated the regional cell status in the right ankle joint. We found that CD11b+MHC II+ cells were increased, but T cells were not increased 3 d after the cytokine injection (Fig. 1 C), suggesting that resident myeloid cells were activated. To investigate cytokine-induced arthritis in the contralateral joint, we injected cytokines into the left ankle and a small concentration of cytokines into the right ankle in both groups. The clinical scores of the right joint were enhanced by the IL-17A and IL-6 injections in the left joint (Fig. 1 D). Thus, sensory pathways were involved in the development of bilateral joint inflammation.

We next examined neural activation after inducing inflammation. Injections of IL-17A and IL-6 induced the expression of c-fos in the ipsilateral L5 DRG but not ipsilateral L3, L4, or L6 DRGs (Fig. 1 E), while c-fos expression was induced in the contralateral L4–L6 DRGs (Fig. 1 F), suggesting that the neural activation induced in the ankle joint transduced through the ipsilateral L5 DRG and contralateral L4–L6 DRGs. The direct neural connection between the ankle joint and DRG was confirmed by detecting a retrograde neural tracer, Fluoro-Gold (FG), which was injected into the right joint. We found that 90.9% of FG+ cells were neurons positive for Nav1.8 but negative for TRPV1. Nav1.8 and TRPV1 double-positive cells were 9.1% of FG+ cells in the L5 DRG (Fig. S1 C). Consistently, activated c-fos+ sensory neurons were Nav1.8+TRPV1− or Nav1.8+TRPV1+ in the contralateral L5 DRG after cytokine injection (Fig. 1, G and H). Thus, ankle-joint inflammation on one side induced Nav1.8+TRPV1− sensory activation in the ipsilateral L5 DRG, and the neural signal subsequently traveled to Nav1.8+TRPV1± sensory neurons on the contralateral side to L4–L6 DRGs, demonstrating that a sensory neural pathway is involved in bilateral ankle joint inflammation.

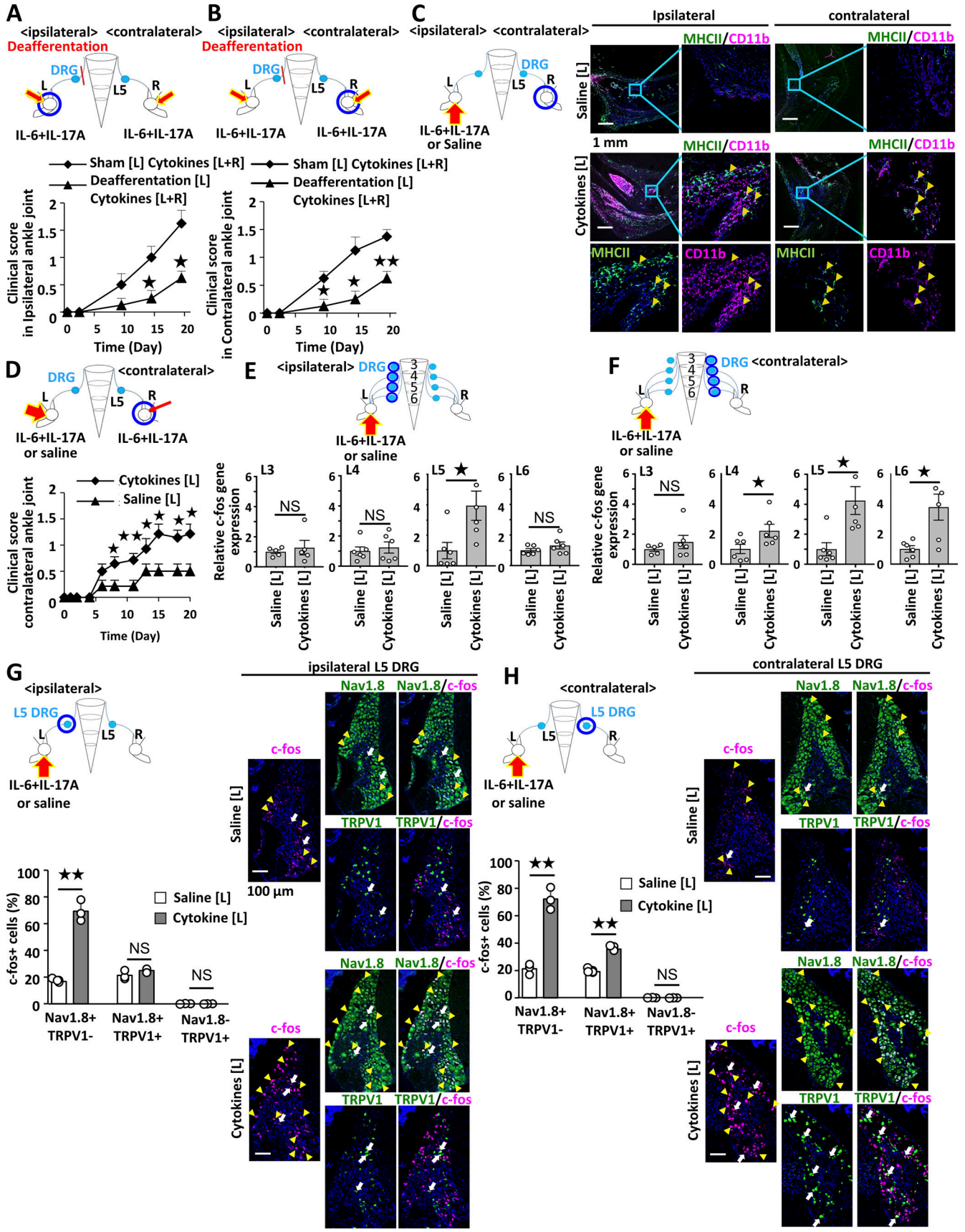

Figure 1. **Activated sensory pathways are involved in bilateral ankle joint inflammation. (A and B)** Clinical scores of the left (A) and right (B) ankles of F759 mice deafferented or sham-operated at L5 DRG of the left side. IL-17A and IL-6 (0.1 µg each) were injected into both ankles on days 0, 1, and 2 (n = 4 per

group). **(C)** CD11b+MHC II+ cells in the ankle joints of F759 mice on day 3 after IL-17A and IL-6 or saline injections. IL-17A and IL-6 or saline (1 µg each) were injected into the left ankle joint on days 0, 1, and 2. Green, MHC II. Magenta, CD11b. Blue, nuclei. Bars, 1 mm. Arrowheads show CD11b+MHC II+ cells. Experiments were performed at least three times independently; representative data are shown. **(D)** Clinical scores of the right ankle joint of F759 mice after IL-17A and IL-6 injections at a low dose (0.01 µg each) in the right ankle joint and high dose (1 µg each) or saline injection in the left ankle joint on days 0, 1, and 2 (n = 14 per group). Mean scores ± SEM are shown. P values were calculated using the Wilcoxon rank-sum test (*, P < 0.05; **, P < 0.01). **(E and F)** IL-17A and IL-6 (1 µg each) or saline was injected into the left ankle joint on days 0, 1, and 2. c-fos expression in ipsilateral (E) or contralateral (F) L3, L4, L5, and L6 DRGs on day 3 using real-time PCR (n = 5–6 per group). **(G and H)** IL-17A and IL-6 (1 µg each) or saline was injected into the left ankle joint on days 0, 1, and 2, followed by staining of c-fos, Nav1.8, and TRPV1 in the ipsilateral (G) or contralateral (H) L5 DRG on day 3. Magenta, c-fos. Green, Nav1.8 or TRPV1. Blue, nuclei. Yellow arrowheads show c-fos+Nav1.8+TRPV1− neurons. White arrows show c-fos+Nav1.8+TRPV1+ neurons. The number of c-fos+, Nav1.8+TRPV1−, Nav1.8+TRPV1+, and Nav1.8−TRPV1+ cells was counted (n = 3 per group). Bar graphs show the percentage of c-fos+ cells in the total number of Nav1.8+TRPV1−, Nav1.8+TRPV1+, or Nav1.8−TRPV1+ neurons. Bar, 100 µm. Experiments were performed three times independently. The data are shown as means ± SEM. P values were calculated using Student's t-tests (*, P < 0.05; **, P < 0.01). Diagrams depicted above or to the left of the graphs illustrate the experimental settings. L, left ankle; R, right ankle. Arrows indicate cytokine or saline injections, and blue circles indicate the ankle joint assessed for arthritis (A–D) or the DRG examined (E–H).

A proenkephalin+ interneuron network connects with sensory neurons between the joints for spreading inflammation

To investigate the neural networks in spinal cord that connect sensory pathways between the ankle joints, we employed herpes simplex virus 2 (HSV2) to trace neural connections regardless of synapses (Turner and Jenkins, 1997). We injected HSV2 into one side of the joint. HSV2 was present in the injected side of L5 DRG on day 4 (Fig. 2 A), reached the dorsal horn of L5 on day 5 (Fig. 2 B), and was detected on the same side of the thoracic cords (T13) by day 7 (Fig. 2 C). It was then detected on the contralateral right side of T10–T13 by day 10 (Fig. 2 D) and in the contralateral DRGs (L4–6) on day 14 (Fig. 2 E and data not shown). These results were confirmed by quantitative PCR (Fig. 2 F). We also investigated whether electrical signals induced activation of the neural circuit in tibial nerves from one side (left side) to the other. An excitatory potential was detected at the contralateral (right) L5 dorsal root (Fig. 2 G), but not at the contralateral tibial nerves (Fig. 2 H). These observations confirmed a neural connection between bilateral ankle joints, at least through both DRGs. Because HSV2 was present on both sides of the thoracic cords at T10–T13, we examined the presence of interneurons connected to sensory pathways between the joints. We performed a lengthwise spinal cord cut in the lower thoracic cords (T9–13) and rested the mice to recover from the surgical operation. The injection of cytokines induced the expression of c-fos in the contralateral L5 DRG in sham-operated mice but only negligibly in the cord-cut mice (Fig. 2 I and Fig. S2 A), suggesting the importance of T9–13 interneurons for spreading inflammation between joints.

We then investigated activated neurons in the spinal cord after cytokine injection in one side of the joints. Phosphorylated c-fos+ neurons were present mainly in the injected side of the L5 dorsal horn at 15 min, and the activated neurons increased in both sides at 30 min (Fig. 2 J). Some neurons around the central canal of the L5 cord were also activated after the cytokine injection (Fig. 2 J). Interestingly, we found activated neurons mainly on the injected side of the T13 dorsal horn but not in T11–T12, L1–L4, or L6 (Fig. 2 K and data not shown). Additionally, neurons around the central canal of the T10 cord were activated 30 min after the stimulation (Fig. 2 L). These results suggested that the neural pathway related to spreading inflammation is a sensory neuron–interneuron connection between the joints.

To investigate interneuron markers involved in spreading inflammation, we employed antibodies against several interneuron markers, including proenkephalin and calretinin (Peirs et al., 2015). We found that most c-fos+ neurons in L5 and T13 expressed proenkephalin but not calretinin after cytokine injection (Fig. 2, M and N). Thus, proenkephalin+ interneuron network connects to sensory neurons between the joints for the spreading inflammation.

Ipsilateral ankle joint inflammation increased ATP in the contralateral ankle joint to trigger inflammation development

We then investigated neurotransmitters in the contralateral ankle joint. Many neurotransmitters are believed to be related to arthritis pathogenesis, including ATP, substance P, calcitonin gene-related peptide (CGRP), and bradykinin (Grassel, 2014; Larsson et al., 1991; Miller et al., 2002; O'Connor et al., 2004; Xie et al., 2014). Indeed, only ATP was increased in the contralateral joint after inflammation induction in the ipsilateral joint (Fig. 3 A). Consistently, ATP synthase expression was increased in Nav1.8+ neurons in the contralateral joint after stimulation (Fig. 3 B). Additionally, NF-κB activation and IL-6 and CCL2 expressions in the contralateral joint were suppressed by the injection of A438079 (a selective P2RX7 antagonist; Fig. 3 C). Finally, the injection of A438079 into the contralateral ankle joint suppressed arthritis development (Fig. 3 D). These results suggest inflammation in the ipsilateral ankle joint increases ATP to induce arthritis in the contralateral joint.

Sensory neuron–interneuron interactions between joints are critical for ATP induction in the contralateral joint

We next investigated functional neural connections between the joints. All of the following events suppressed ATP induction in the contralateral joint after cytokine injections into the other joint: the deafferentation of sensory neurons at L5 DRG on the cytokine-injected side (Fig. 3 E); a lengthwise T9–13 spinal cord cut (Fig. 3 F); and the deafferentation of contralateral L4–L6 DRG sensory nerves (Fig. 3 G). These results suggest that functional sensory neuron–interneuron connections exist between the ankle joints and are sufficient for ATP induction in the contralateral ankle joint.

Regional ATP is induced by ipsilateral joint inflammation and functions as a neurotransmitter to develop contralateral joint inflammation

Next, we examined how ipsilateral joint inflammation activates sensory neurons. Because we previously found that extracellular

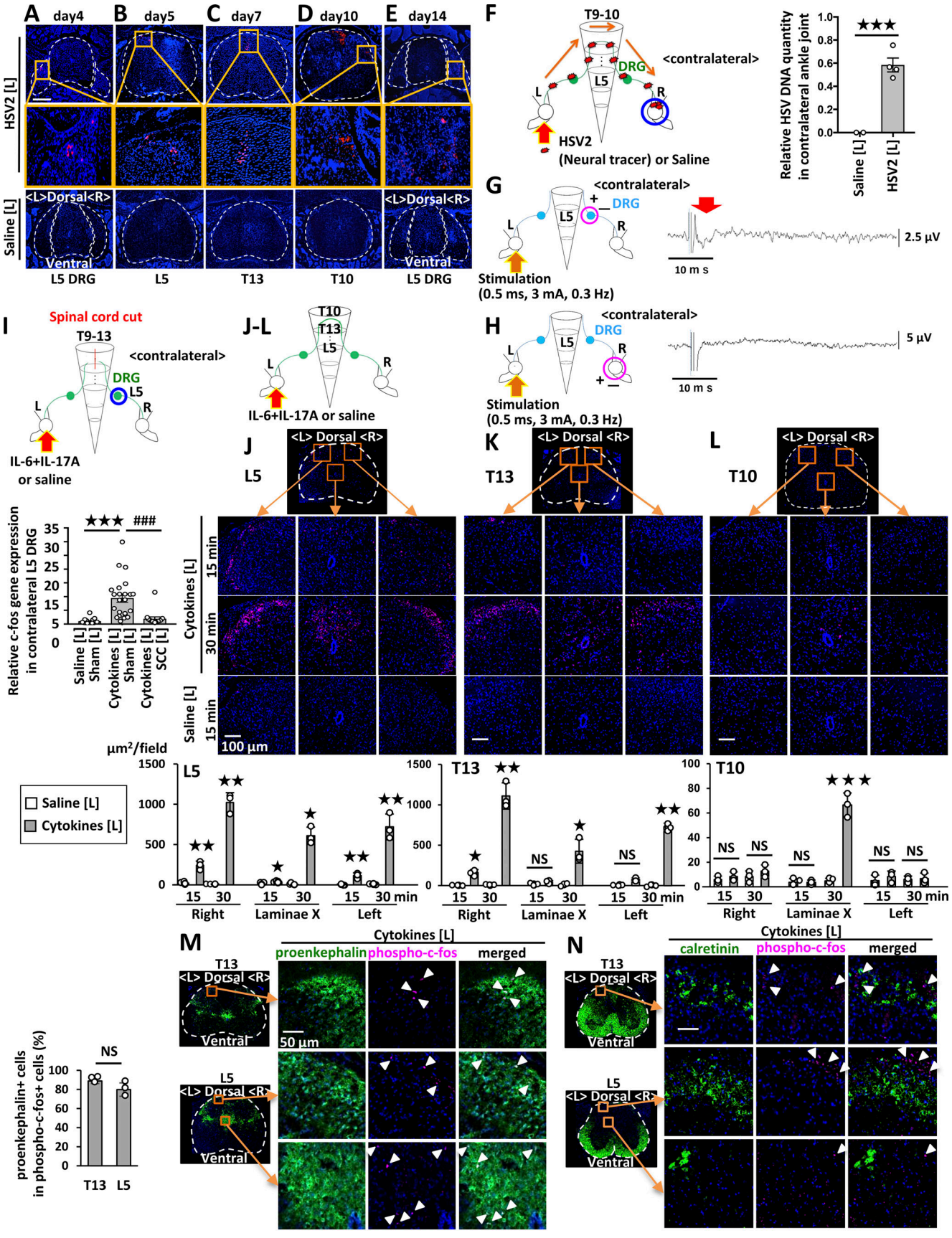

Figure 2. **Cytokine injections into the ankle joints activate neural pathways including proenkepharin+ interneurons in the spinal cord between bilateral joints. (A–E)** HSV2 (4.5 × 105 pfu) or saline was injected into the left ankle joint of F759 mice, followed by staining of HSV2 in the spinal cord and L5

DRG on day 4 (A), L5 on day 5 (B), T13 on day 7 (C), T10 on day 10 (D), and L5 DRG on day 14 (E). Nuclear staining by Hoechst 33342 is shown in blue. Broken lines outline the spinal cord and DRG. Magnified images in the orange boxes are shown in the middle row. Sections from control F759 mice given saline injection are shown at the bottom. Experiments were performed at least three times independently; representative data are shown. **(F)** HSV2 (4.5 × 105 pfu) or saline was injected into the left ankle joints of F759 mice on day 0, followed by the detection of HSV2 DNA in the contralateral (right) ankle joint on day 20 by real-time PCR (n = 2–4 per group). **(G and H)** An electrical stimulation (0.5 ms, 3 mA, 0.3 Hz) was applied to the left tibial nerves. Electrical signals were detected at the dorsal root (G) or tibial nerve levels (H) on the contralateral (right) side (n = 5 per group). The red arrow shows the electrophysiological signal detected. As a positive control, stimuli were applied to the nerve on the recording (right) side, and compound action potentials were detected at the dorsal root and sciatic nerve levels (not shown). **(I)** c-fos expression of the right L5 DRG in F759 mice who underwent a spinal cord cut (SCC; T9–T13) or sham operation. IL-17A and IL-6 (1 µg each) or saline were injected into the left ankle on days 0, 1, and 2, and c-fos expression was examined by real-time PCR on day 3 (n = 15–23 per group). Mean scores ± SEM are shown. P values were calculated using Student's t-tests (F) and Dunnett's test (I; *** and ###, P < 0.001). Diagrams illustrate the experimental settings. L, left ankle; R, right ankle. Arrows indicate HSV2, cytokine, or saline injections. Blue circles indicate the ankle or DRG examined. **(J–L)** IL-17A and IL-6 (1 µg each) or saline was injected into the left ankle joint of F759 mice on day 0, followed by the analysis of phosphorylated c-fos expression in the L5 spinal cord (J), T13 spinal cord (K), and T10 spinal cord (L) 15 or 30 min after the last injection. Magenta, phosphorylated-c-fos; Blue, nuclei. Bar, 100 µm. Phosphorylated c-fos positive areas per field (225,625 µm^2) were quantified (n = 3 per group). **(M and N)** IL-17A and IL-6 (1 µg each) or saline was injected into the left ankle joint of F759 mice on day 0, followed by the analysis of phosphorylated c-fos and proenkephalin (M) or calretinin (N) expression in the L5 and T13 spinal cord 15 min after the last injection. Green, proenkephalin (M) or calretinin (N). Magenta, phosphorylated c-fos. Blue, nuclei. Bar, 50 µm. Arrowheads show phosphorylated c-fos signals. Experiments were performed three times independently; representative data are shown. Mean scores ± SEM are shown. P values were calculated using Student's t-test or Welch's t-test (J–L; *, P < 0.05, **, P < 0.01, ***, P < 0.001). Diagrams illustrate the experimental settings. L, left ankle; R, right ankle. The arrows indicate cytokine or saline injection.

ATP induced from regional blood vessels by cytokine stimulation enhances the activation of a neural pathway in the brain (Arima et al., 2017), we focused our attention on ATP. ATP concentration increased after IL-17A and IL-6 stimulation in synovial cells in a manner dependent on NF-κB activation in vitro (Fig. 3 H). Moreover, ATP concentration significantly increased in the ankle joint after cytokine injections in a manner dependent on Col1a+ non-immune cells (Fig. 3 I). The injection of IL-6 and IL-17A plus A438079 in one ankle joint suppressed the neural activation of L5 DRG neurons (Fig. 3 J) and increased the ATP concentration in the other joint (Fig. 3 K). Furthermore, the injection of ATP in one ankle joint increased ATP concentration in the contralateral joint (Fig. 3 L). Additionally, ATP injection in one ankle joint of WT mice activated neurons in L5 DRG on the ipsilateral side and L4–L6 DRGs on the contralateral side (Fig. S2 B), which resembles the neural status observed in F759 mice after stimulation (Fig. S2 A). ATP injection also activated neurons in L5, T13, and T10 spinal cords (Fig. S2 C). On the other hand, neural activation in the contralateral DRGs of WT mice was suppressed by a spinal cord cut, which is also consistent with F759 mice (Fig. S2, A and B). Neural activation was confirmed by a targeted recombination in active populations system, in which tdTomato is expressed under the control of the c-fos promoter (Fig. S2 D). Thus, we confirmed a neural connection between bilateral ankle joints through both DRGs and the lower thoracic cord in F759 mice and WT mice after cytokine stimulation in one joint.

We then examined whether blockade of the ATP signal suppresses spreading inflammation in a cytokine-injected joint. Arthritis development was suppressed by the injection of A438079 into the same joint in F759 mice (Fig. 3 M). Importantly, the unilateral injection of A438079 suppressed the development of bilateral arthritis (Fig. 3, N and O). Thus, cytokine stimulation in Col1a+ non-immune cells increases ATP expression to activate sensory pathways in the ankle joint, causing spreading inflammation.

ATP is secreted by NF-κB activation and a critical NF-κB stimulator in the contralateral joint

The importance of the ATP–P2RX7 axis on immune cell function has been reported (Labasi et al., 2002). Here, we investigated the effects of the ATP–P2RX7 axis on non-immune cells, including sensory neurons, endothelial cells, and fibroblasts, in the contralateral joint. ATP injection in the unilateral joint did not increase ATP in the contralateral side in F759 mice deficient in NF-κB or STAT3 signaling in Col1a+ non-immune cells (Fig. 3 P), suggesting that the IL-6 amplifier is critical for the increase of ATP in the contralateral joint. We also found that vimentin+ cells, including synovial fibroblastic cells and endothelial cells, had phosphorylated NF-κB and STAT3 molecules in the contralateral joint after stimulation (Fig. 3 Q). Importantly, blockade of P2RX7 signaling by A438079 abrogated the contralateral ATP increase (Fig. 3 R). P2RX7 was expressed by vimentin+ and/or CD31+ cells, as well as by Nav1.8+ neurons regardless of the stimulation (Fig. 3 S). Phosphorylated CAMP responsive element binding protein 1 (CREB) molecules, which are ATP signaling targets, were increased in vimentin+ cells and CD31+ cells in the contralateral joint after stimulation (Fig. S3 A). These results suggest that synovial fibroblasts and endothelial cells in contralateral joints are responder cells to ATP. Thus, these non-immune cells secrete IL-6 and CCL2 as well as more ATP in a manner dependent on the IL-6 amplifier in the contralateral joint.

A similar mechanism occurs in CIA

We investigated whether our observations in the F759 model could be applied to conventional RA models. Accordingly, we employed the CIA model and found that intra-articular injections of A438079 suppressed the development of joint inflammation (Fig. 4 A), as did the intra-articular injections of an anti–IL-6R and anti–IL-17A antibodies (Fig. 4 B), suggesting that this model is locally ATP/NF-κB/STAT3 dependent. Moreover, ATP levels in the joint increased during CIA (Fig. 4 C). A lengthwise T9–13 spinal cord cut suppressed ATP induction in the ankle joint and the development of bilateral ankle arthritis (Fig. 4, D and E). Furthermore, unilateral intra-articular injections of A438079 suppressed the bilateral joint inflammation (Fig. 4 F). The direct injection of ATP in one ankle joint increased the ATP concentration in the other joint of WT mice even without CIA (Fig. S3 B). Thus, the sensory neuron–interneuron pathway identified in the cytokine-induced arthritis model is

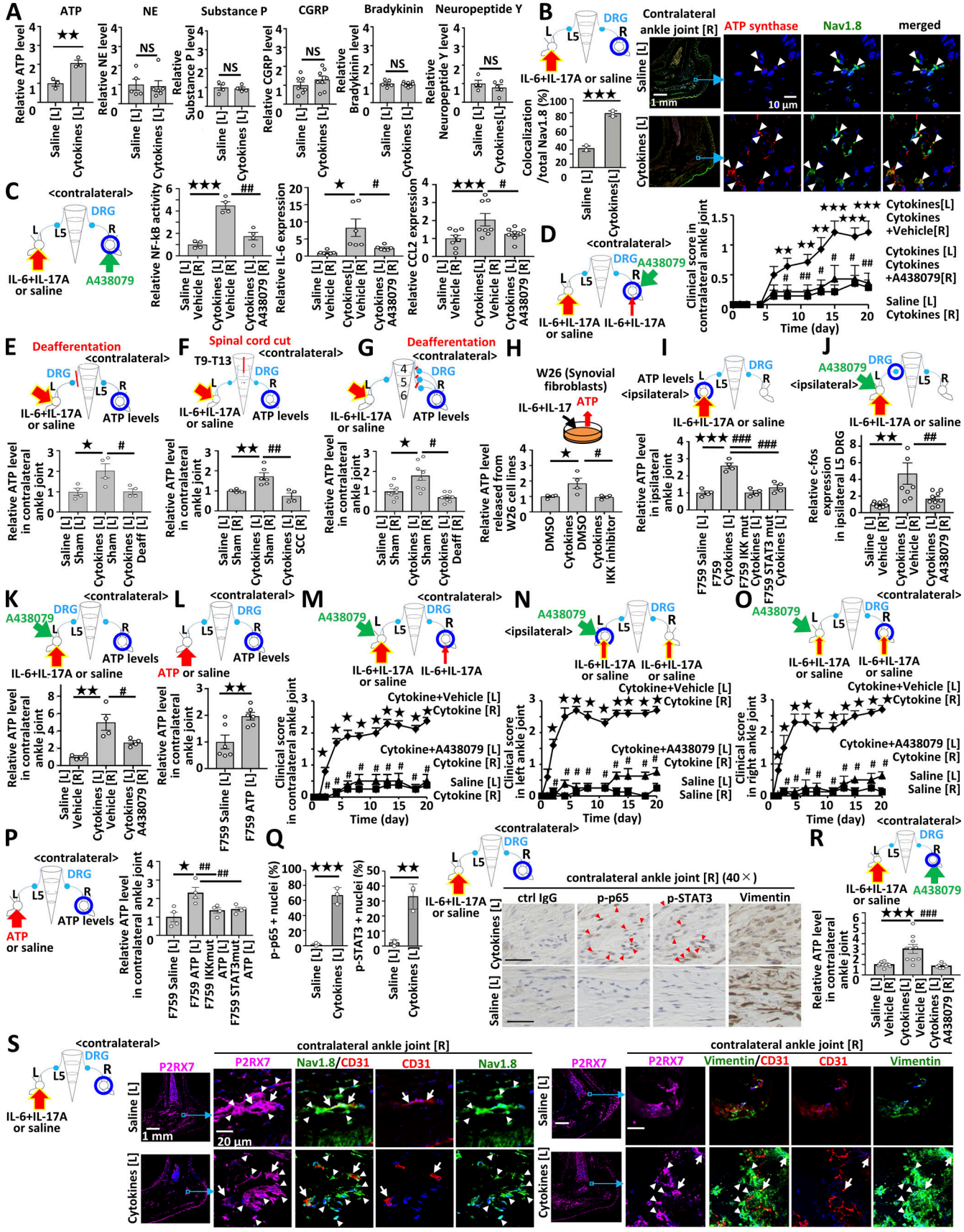

Figure 3. **ATP from non-immune cells mediates the conversion of IL-17A and IL-6 cytokine signals into neural activation to induce remote inflammation. (A)** IL-17A and IL-6 (1 µg each) or saline was injected into the left ankle joints of F759 mice on days 0, 1, and 2, followed by the analysis of ATP (*n* =

3 per group), norepinephrine (NE; *n* = 5–6 per group), substance P (*n* = 4 per group), CGRP (*n* = 7–8 per group), bradykinin (*n* = 5–8 per group), and neuropeptide Y (*n* = 4–5 per group) levels in the contralateral (right) ankle joint on day 3. Graphs show the relative expression level against the saline-injected group. **(B)** IL-17A and IL-6 (1 µg each) or saline were injected into the left ankle joints of F759 mice on days 0, 1, and 2, followed by immunostaining for ATP synthase and Nav1.8 in the contralateral (right) ankle joint on day 3. The colocalization of ATP synthase and Nav1.8 was quantified using Z-stack images (*n* = 3 per group). The bar graph shows the percentage of the colocalized signal volume in the total signal volume of Nav1.8. Red, ATP synthase. Green, Nav1.8. Blue, nuclei. Arrowheads show merged signals. Bars, 1 mm or 10 µm. **(C)** IL-17A and IL-6 (1 µg each) or saline were injected into the left ankle joint of F759 mice on days 0, 1, and 2 in the presence or absence of A438079 in the contralateral (right) ankle joint, followed by the analysis of NF-κB activation and IL-6 and CCL2 levels in the contralateral ankle joint on day 3 (*n* = 4–6 per group). **(D)** IL-17A and IL-6 (1 µg each) or saline were injected into the left ankle joint, and a low dose of IL-17A and IL-6 (0.01 µg each) with A438079 (10 µg) was injected into the right ankle joint of F759 mice on days 0, 1 and 2. Clinical arthritis scores of the right ankle joint were evaluated (*n* = 4–5 per group). Mean scores ± SEM are shown. P values were calculated using Student's *t*-tests (A–C) and the Wilcoxon rank-sum test (D; * and #, P < 0.05; ** and ##, P < 0.01; ***, P < 0.001). Diagrams illustrate the experimental settings. L, left ankle; R, right ankle. Arrows indicate cytokine, saline, or A438079 injections. Blue circles indicate the ankle joints examined. **(E)** IL-17A and IL-6 (1 µg each) or saline were injected into the left ankle joint of F759 mice deafferented (Deaff) or sham-operated (Sham) at the L5 DRG of the left side on days 0, 1, and 2, followed by the analysis of ATP levels in the contralateral (right) ankle joint on day 3 using an ATP assay kit (*n* = 4 per group). **(F)** IL-17A and IL-6 (1 µg each) or saline were injected into the left ankle joint of F759 mice with a lengthwise T9-13 spinal cord cut (SCC) or sham-operated (Sham) on days 0, 1, and 2, followed by the analysis of ATP levels in the contralateral (right) ankle joint on day 3 (*n* = 4–6 per group). **(G)** IL-17A and IL-6 (1 µg each) or saline was injected into the left ankle joint of F759 mice deafferented (Deaff) at the L4–L6 DRGs of the right side or sham-operated (Sham) on days 0, 1, and 2, followed by the analysis of ATP levels in the contralateral (right) ankle joint on day 3 (*n* = 8 per group). Experiments were performed at least three times independently; representative data are shown. Mean scores ± SEM are shown. P values were calculated using Dunnett's test (* and #, P < 0.05; ** and ##, P < 0.01). Diagrams illustrate the experimental settings. L, left ankle; R, right ankle. Arrows indicate cytokine or saline injections. Blue circles indicate the ankle joints examined. **(H)** W26 synovial fibroblasts were stimulated with human IL-6 (50 ng/ml) plus soluble IL-6Rα (50 ng/ml) and mouse IL-17A (50 ng/ml) with or without IKK2 inhibitor IV (5 µM). Culture supernatants were collected and assessed using an ATP assay kit (*n* = 4 per group). **(I)** IL-17A and IL-6 (1 µg each) or saline were injected into the left ankle joint of F759 mice, F759/Col1α-cre IKKγflox/flox mice, and F759/Col1α-cre STAT3flox/flox mice on days 0, 1, and 2, followed by the analysis of ATP concentration in the ipsilateral (left) ankle joint on day 3 (*n* = 4 per group). **(J)** IL-17A and IL-6 (1 µg each) or saline were injected with or without the P2RX7 inhibitor A438079 into the left ankle joint of F759 mice on days 0, 1, and 2, followed by the analysis of c-fos expression in the ipsilateral (left) L5 DRG on day 3 (*n* = 8–9 per group). **(K)** IL-17A and IL-6 (1 µg each) or saline were injected with or without A438079 into the left ankle joint of F759 mice on days 0, 1, and 2, followed by the analysis of ATP concentration in the contralateral (right) ankle joint on day 3 (*n* = 4 per group). **(L)** ATP (2 µg) or saline was injected into the left ankle joint of F759 mice on days 0, 1, and 2, followed by the analysis of ATP concentration in the contralateral (right) ankle joint on day 3 (*n* = 6 per group). Mean scores ± SEM are shown. P values were calculated using Dunnett's test (H–K) and Student's *t*-test (L; * and #, P < 0.05; ** and ##, P < 0.01; *** and ###, P < 0.001). Diagrams illustrate the experimental settings. L, left ankle; R, right ankle. Arrows indicate cytokine, saline, or ATP injections. Blue circles indicate the ankle joints or DRG examined. **(M)** IL-17A and IL-6 (1 µg each) or saline were injected into the left ankle joint, and a low dose of IL-17A and IL-6 (0.01 µg each) were injected into the right ankle joint with or without A438079 (10 µg) into the left ankle joint of F759 mice on days 0, 1 and 2. Clinical arthritis scores of the right ankle joint of F759 mice were evaluated (*n* = 14 per group). **(N and O)** Clinical arthritis scores from the left (N) or right (O) ankle joint of F759 mice after injections of IL-17A and IL-6 (0.1 µg each) in both ankle joints on days 0, 1, and 2 with or without A438079 (10 µg; *n* = 4–5 per group). Mean scores ± SEM are shown. P values were calculated using the Wilcoxon rank-sum test (* and #, P < 0.05). Diagrams illustrate the experimental settings. L, left ankle; R, right ankle. Arrows indicate cytokine, saline, or A438079 injections. Blue circles indicate the ankle joints examined. **(P)** ATP (2 µg) or saline was injected into the left ankle joint of F759 mice, F759/Col1α-cre IKKγflox/flox mice, and F759/Col1α-cre STAT3flox/flox mice on days 0, 1, and 2, followed by the analysis of ATP concentration in the contralateral (right) ankle joint on day 3 (*n* = 4 per group). **(Q)** IL-17A and IL-6 (1 µg each) or saline was injected into the left ankle joint of F759 mice on days 0, 1, and 2, followed by the detection of phosphorylated NF-κB p65 (p-p65) and STAT3 (p-STAT3), and vimentin (non-immune cell marker) in the contralateral (right) ankle joint by immunohistochemistry. Arrowheads show p-p65+ or p-STAT3+ nuclei. Bar graphs shows the percentage of p-p65+ or p-STAT3+ nuclei in the total nuclei (*n* = 3 per group). Bar, 20 µm. **(R)** IL-17A and IL-6 (1 µg each) or saline were injected into the left ankle joint with or without A438079 injection into the right ankle joint of F759 mice on days 0, 1, and 2, followed by the analysis of ATP levels in the contralateral (right) ankle joint on day 3 (*n* = 7–10 per group). **(S)** IL-17A and IL-6 (1 µg each) or saline were injected into the left ankle joint of F759 mice on days 0, 1, and 2, followed by immunostaining for P2RX7, Nav1.8, vimentin, and CD31 in the contralateral (right) ankle joint on day 3. Magenta, P2RX7. Green, Nav1.8 or vimentin. Red, CD31. Blue, nuclei. Arrows show P2RX7 signals merged with Nav1.8+CD31+ or vimentin+CD31+ signals. Arrowheads show P2RX7 signals merged with Nav1.8 or vimentin signals. Bars, 1 mm or 20 µm. Experiments were performed at least three times independently; representative data are shown. Mean scores ± SEM are shown. P values were calculated using Dunnett's test (P, R, and S) or Student's *t*-test (Q; *, P < 0.05; ** and ##, P < 0.01; *** and ###, P < 0.001). Diagrams illustrate the experimental settings. L, left ankle; R, right ankle. Arrows indicate cytokine, ATP, saline, or A438079 injections. Blue circles indicate the ankle joints examined.

also present in WT mice and contributes to the pathogenesis of bilateral ankle inflammation in the CIA model.

We show a mechanism for spreading inflammation between ankle joints in cytokine-induced and CIA models (Fig. 5). Sensory neurons that distribute around the ankle joints mainly connected to L5 DRG but also L4 and L6 DRGs (Kawano et al., 2004). Consistently, cytokine injections into one ankle joint of F759 mice induced c-fos expression on both sides of L5 DRG, suggesting that the inflammation signal from one side activates sensory neurons in both sides. Our results indicate that ATP from non-immune cells is a key neurotransmitter for activating sensory pathways toward the contralateral joint. We also found that ATP is released from sensory neurons with ATP synthase in the contralateral joint. Interestingly, endothelial cells (Arima et al., 2017) and synovial cells (Fig. 3 H) also produced ATP after cytokine stimulations, and ATP stimulated IL-6 amplifier activation. Therefore, we hypothesized that ATP is both a key neurotransmitter and inflammation mediator in both joints.

Spreading inflammation is common in RA. Lefevre et al. (2009) showed that RA synovial fibroblasts (RASFs) are able to migrate and contribute to the spread of the disease. However, how RASFs reach the other joints remains to be elucidated. We hypothesized that the local neural regulation for bilateral inflammation shown here triggers chemokine expression and promotes the subsequent recruitment of RASFs. Donaldson et al. reported that capsaicin-sensitive TRPV1+ fibers are involved in the spread of inflammation to the contralateral side using CFA-induced arthritis (Donaldson et al., 1995). Our data also suggest

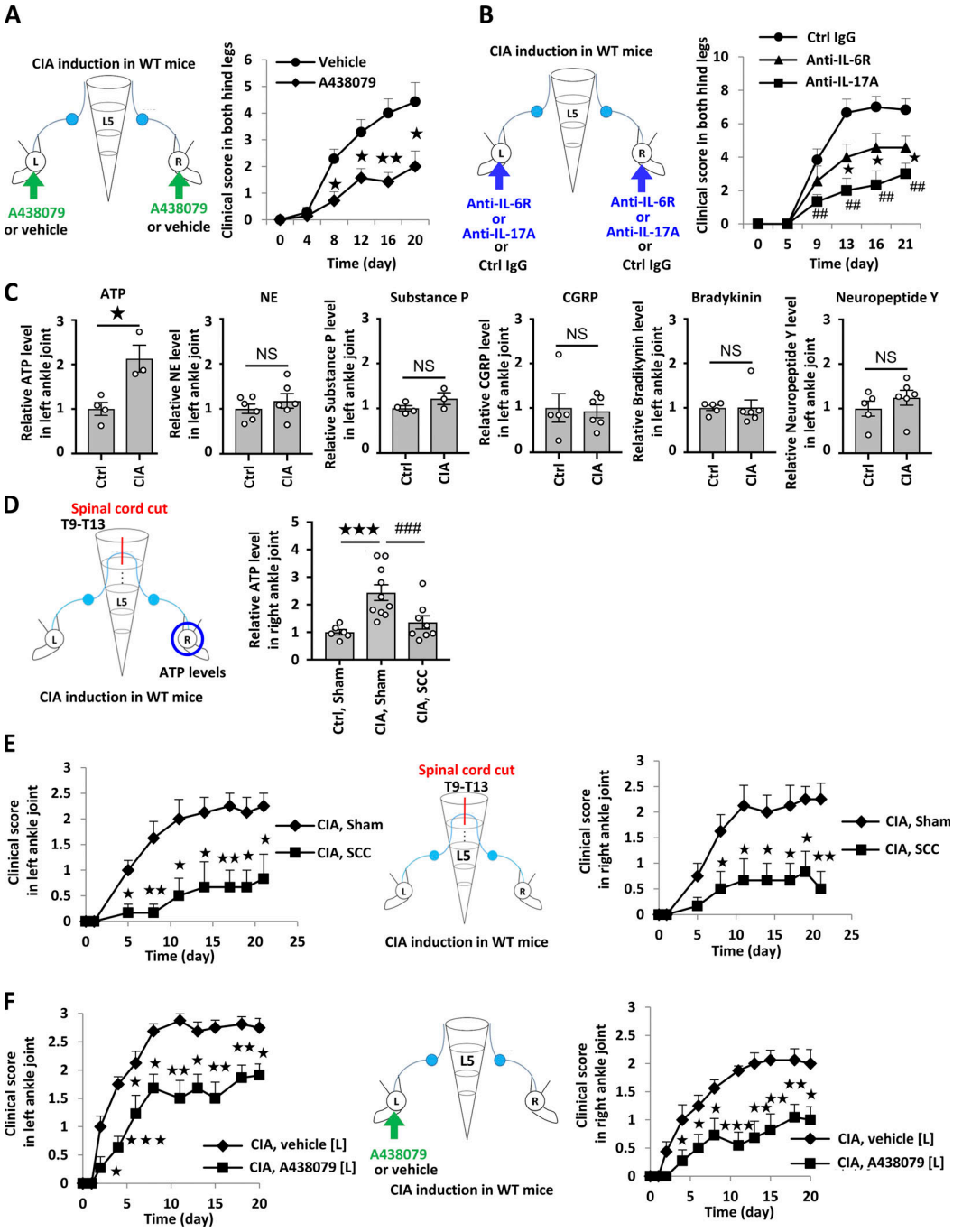

Figure 4. **ATP induces sensory pathway between bilateral joints in WT mice during CIA. (A)** CIA was induced in C57BL/6 mice. Clinical scores from both hind legs of CIA mice that received bilateral injections of A438079 every day from days 4–28 after primary immunization (n = 7 per group). **(B)** Clinical arthritis scores from both hind legs of CIA mice that received bilateral injections of anti–IL-6R antibody (2 µg), anti–IL-17A antibody (2 µg), or control antibody every day from days 14–28 after primary immunization (n = 7 per group). **(C)** CIA was induced in C57BL/6 mice, followed by the analysis of ATP, norepinephrine (NE), substance P, CGRP, bradykinin, and neuropeptide Y levels in the right ankle joint on day 23 after primary immunization (n = 4–6 per group). Graphs show the relative expression level against the saline-injected group. **(D)** CIA was induced in C57BL/6 mice after a lengthwise T9–13 spinal cord cut (SCC) or sham-operation (Sham), followed by the analysis of ATP levels in the right ankle joint on day 23 after primary immunization (n = 5–10 per group). **(E)** Clinical arthritis scores from the left or right ankle joint after a lengthwise T9–13 spinal cord cut (SCC) or sham-operation (Sham; n = 9–10 per group). **(F)** Clinical arthritis scores from the left or right ankle joint of CIA mice that received unilateral injections of A438079 or vehicle every day from days 14–28 in the left ankle joint (n = 9–10 per group). Mean scores ± SEM are shown. P values were calculated using the Wilcoxon rank-sum test (A, B, E, and F), Student's t-test (C), and Dunnett's test (D; *, P < 0.05; ** and ##, P < 0.01; *** and ###, P < 0.001). Diagrams illustrate the experimental settings. L, left ankle; R, right ankle. Arrows indicate A438079, vehicle, or antibody injections. Blue circles indicate the ankle joints examined.

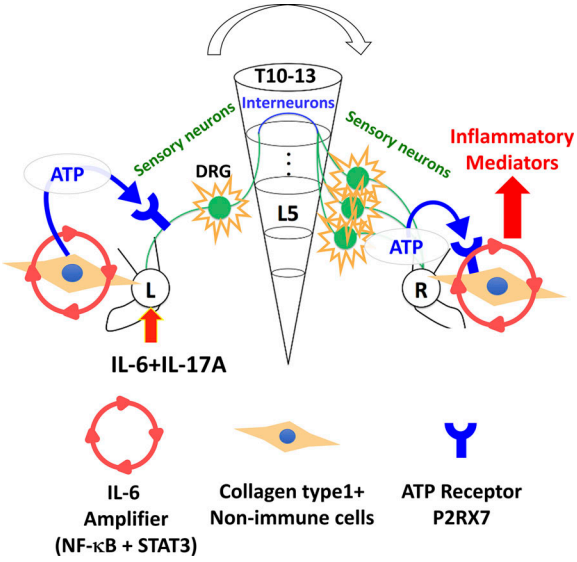

Figure 5. **A schematic model for spreading inflammation.** ATP induced by activation of the IL-6 amplifier in Col1a+ non-immune cells in one side of the ankle joint (left side) activates Nav1.8+TRPV1± sensory neurons, which stimulate the regional sensory neural pathway involving the lower thoracic spinal cord that contains proenkephalin+ interneurons. On the contralateral side (right side), the response of sensory neurons in L4–L6 DRGs releases ATP, which induces inflammatory mediators, including cytokines and chemokines, by activating the IL-6 amplifier in Col1a+ non-immune cells, including fibroblasts and endothelial cells, through P2RX7.

the involvement of Nav1.8+TRPV1± sensory neurons in F759 arthritis. In CFA-induced arthritis, the anterior cingulate cortex could be the site from which inflammation spreads to the contralateral side (Arima et al., 2017), which suggests a different mechanism from that in the F759 model. Further study is required to determine the detailed relationship between each neural circuit during spreading inflammation.

We examined whether circulating cytokine levels during F759 arthritis contributed to the disease development. Mouse IL-6 levels in serum were equivalent between cytokine-injected and non-injected mice, indicating no major systemic inflammatory responses were induced (Fig. S3 C). On the other hand, increased circulating levels of human IL-6 and mouse IL-17A were detected after the cytokine injections (Fig. S3 C), suggesting that a small level of cytokines was systemically absorbed. However, these concentrations were too low to activate the IL-6 amplifier in vitro and hardly contributed to the cytokine-induced arthritis in vivo (Fig. S3, D and E). Thus, circulating cytokines did not affect contralateral ankle joint inflammation after cytokine injection at the ipsilateral side.

ATP is known to be released both from non-immune cells and sensory neurons (Arima et al., 2017; Holton, 1959) and has neurotransmitter activity (Burnstock, 2006). We hypothesized that ATP in the ipsilateral joint is not only an inflammation mediator but also a neurotransmitter for sensory pathways. On the other hand, in the contralateral joint, sensory neurons produced ATP to activate the IL-6 amplifier in non-immune cells, which produced more ATP and IL-6. Namely, in the ipsilateral joint, the IL-6 amplifier triggered ATP secretion to stimulate the sensory pathway that connects to the contralateral joint. The resulting ATP activated the IL-6 amplifier to secrete more IL-6 and ATP in the contralateral joint. Consistently, the blockade of ATP signaling in the contralateral joints suppressed the contralateral ATP increase. Thus, positive feedback between the ATP and IL-6 secreted by non-immune cells contributes to the inflammation development in the contralateral joint.

Our findings suggest that a proenkephalin+ interneuron network establishes the neural circuit between joints that regulates spreading inflammation via sensory pathways. Sensory neurons in DRGs have an antidromic function called the axon reflex and contribute to regional inflammation (Chavan et al., 2017). We hypothesized that Nav1.8+ sensory neurons in the ipsilateral L5 DRG might be responsible for the orthodromic propagation of action potentials to the spinal cord and sensory neurons in contralateral L4–L6 DRGs are involved in the antidromic axon reflex, exacerbating the contralateral joint inflammation (Chavan et al., 2017). Because electrophysiology assays showed that anterograde neural activation is stronger than antidromic neural activation (Sorkin et al., 2018), we performed such assays on mice by electrically stimulating the sciatic nerves. We detected an electrophysiological signal in the ipsilateral side, as expected (data not shown), and around the contralateral DRG (Fig. 2 G). This finding is consistent with the antidromic sensory neural pathway being involved in the contralateral ankle joint inflammation in our system.

To conclude, we report a mechanism of spreading inflammation in two arthritis models. We show that a regional sensory neuron–interneuron connection between the joints through the thoracic spinal cord is critical for spreading inflammation via ATP, which activates a neural pathway and enhances the IL-6 amplifier. While future study is required to determine if the same mechanism applies to spreading inflammation in RA patients and other models, blockade of this neural pathway, which we named as the spreading gateway reflex, may be a therapeutic target for various diseases with spreading inflammation.

Materials and methods

Mouse strains

C57BL/6 mice were purchased from Japan SLC. F759 mice were backcrossed with C57BL/6 mice for more than 10 generations. Adult (8–10 wk of age) male mice were used in all experiments. Type I collagen–Cre mice were provided by Dr. G. Karsenty (Baylor College of Medicine, Houston, TX) and crossed with STAT3flox/flox mice (provided by Dr. S. Akira, Osaka University, Osaka, Japan; Takeda et al., 1998) and IKKγflox/flox mice (Schmidt-Supprian et al., 2000). NF-κB–reporter transgenic mice in a C57BL/6 background were also backcrossed with F759 mice and used (Sadikot and Blackwell, 2008). B6.129(Cg)-Fos$^{tm1.1(cre/ERT2)Luo}$/mice and B6;129S6-Gt(ROSA)26Sortm14(CAG-tdTomato)Hze/J (Ai14) mice were purchased from The Jackson Laboratory and crossed to obtain c-fos CreERT2-Ai14 mice. The mice were maintained under specific pathogen–free conditions according to the protocols of Osaka University Medical School. All animal experiments were performed following the guidelines of the Institutional Animal Care and Use Committees of the

Graduate School of Frontier Biosciences and Graduate School of Medicine, Osaka University, and the Institute for Genetic Medicine, Hokkaido University. The protocols for animal experiments were approved by the Institutional Animal Care and Use Committees of the Graduate School of Frontier Biosciences and Graduate School of Medicine, Osaka University, and Hokkaido University.

Antibodies and reagents

The following antibodies were used for staining: anti–c-Fos rabbit polyclonal antibodies (product no. ab190289; Abcam), anti-Nav1.8 rabbit polyclonal antibodies (a gift from Dr. Watanabe), anti-phosphorylated-c-fos (Ser32) rabbit monoclonal antibody (D82C12; no. 5368S; Cell Signaling Technologies), anti-HSV2 rabbit whole antisera (no. NB120-9534; Novus Biologicals), anti-pro-enkephalin guinea pig polyclonal antibodies (a gift from Dr. M. Watanabe), anti-TRPV1 guinea pig polyclonal antibodies (a gift from Dr. M. Watanabe), anti-calretinin chicken polyclonal antibodies (no. CPCA-Calret; Encor Biotechnology), anti-phosphorylated STAT3 (Tyr705) rabbit monoclonal antibody (D3A7; no. 9145; Cell Signaling Technologies), anti-vimentin (no. ab92547; Abcam), anti-phosphorylated NF-κB p65 (pSer^{276}) rabbit polyclonal antibodies (no. SAB4504488; Sigma-Aldrich), anti-P2RX7 goat polyclonal antibodies (no. ab93354; Abcam), anti-mouse CD31 rat monoclonal antibody (no. 550274; BD Pharmingen), Alexa Fluor 647 labeled anti-phosphorylated CREB (Ser133) rabbit monoclonal antibody (clone 87G3, no. 14001S; Cell Signaling Technologies), Alexa Fluor 546 donkey anti-rabbit IgG (H + L; no. A10040; Thermo Fisher Scientific), Alexa Fluor 488 donkey anti-rabbit IgG (H + L; no. A21206; Thermo Fisher Scientific), Alexa Fluor 555 donkey anti-rabbit IgG (H + L; no. A31572; Thermo Fisher Scientific), Alexa Fluor 488 donkey anti-goat IgG (H + L; no. A11055; Thermo Fisher Scientific), Alexa Fluor 647 goat anti-chicken IgG (H + L; no. A21449; Thermo Fisher Scientific), Alexa Fluor 488 donkey anti-guinea pig IgG (H + L; no. 756-545-148; Jackson ImmunoResearch), and Alexa Fluor 555 donkey anti-rat IgG (H + L; no. ab150154; Abcam). VECTASTAIN Elite ABC Kit Peroxidase (Rabbit IgG) and ImmPACT DAB Substrate Kit Peroxidase were purchased from Vector Laboratories. Anti-mouse IL-17 Ab (no. MAB421; R&D Systems) and anti-IL-6R Ab (Chugai Pharmaceutical Co.) were used for in vivo neutralization. Mouse IL-17A was purchased from Peprotech. Human soluble IL-6Rα was purchased from R&D systems. Human IL-6 was obtained from Toray Industries. A438079 hydrochloride (no. 2972), A803467 (no. 2976), and IKK 16 (no. 2539) were purchased from Tocris Bioscience. FG was purchased from Fluorochrome (no. 52-9400), and ATP from Sigma-Aldrich (no. A6559). ATP Measuring Reagent Kit was purchased from TOYO Ink (no. LL100-1), Bradykinin EIA Kit (Human, Rat, Mouse; no. EK-009-01) and CGRP EIA Kit (Rat, Mouse; no. EK-015-09) from Phoenix Pharmaceuticals, Human IL-6 ELISA Set (no. 555220) from BD Biosciences, IL-17 mouse ELISA (no. BMS6001) from Thermo Fisher Scientific, LEGEND MAX Human IL-6 ELISA Kit (no. 430507) from BioLegend, Luciferase reporter assay system (no. E1500) from Promega, and Norepinephrine EIA Kit (no. VA-10-0200) from LDN. Alexa Fluor-488– (no. C22841) and Alexa Fluor-555– (no. C22843) conjugated cholera toxin B subunit, Zenon Rabbit IgG Labeling Kit, Alexa Fluor 488 (no. Z25302), and Alexa Fluor 555 (no. Z25305) were purchased from Thermo Fisher Scientific.

Joint injections

IL-6, IL-17A, ATP, A803467, A438079, FG, HSV2 (no. VR-540; ATCC), Alexa Fluor labeled cholera toxin B subunit, anti-mouse IL-17 antibody, and anti–IL-6R antibody were injected into the ankle and knee joints of mice as described previously (Atsumi et al., 2017; Harada et al., 2015; Meng et al., 2016; Murakami et al., 2013; Murakami et al., 2011).

Clinical assessment of cytokine-induced arthritis

F759 mice injected with IL-6 and IL-17A were assessed for signs of arthritis as described previously (Atsumi et al., 2017; Harada et al., 2015; Meng et al., 2016; Murakami et al., 2013; Murakami et al., 2011). Briefly, the severity of the arthritis was based on two bilaterally assessed parameters: (1) swelling of the ankle and (2) restricted mobility of the ankle joints. The severity of each parameter was graded on a scale of 0–3, where 0 indicates no change; 1, mild change; 2, medium change; and 3, severe change. Averages for a single point in one leg ankle joint from each mouse were used.

Deafferentation

Deafferentation was conducted as described previously (Kawano et al., 2007). Briefly, a skin incision was made along the vertebra between the thoracic-to-sacral level, the left dorsal root of the spinal cord at the L4–5 segmental levels or L4–6 segment levels was exposed, and the afferent fibers between the spinal cord and DRGs at L5 or L4–L6 were transected. Mice in the sham-operated control group had their left DRGs and roots exposed, but the nerve supply was kept intact. The contralateral side was kept intact for all mice. 14 d of ambulation were allowed after the surgery.

Partial sciatic nerve ligation

Partial sciatic nerve ligation (Seltzer model) was performed as described previously (Malmberg and Basbaum, 1998; Seltzer et al., 1990). Briefly, a skin incision was made on the hip and the sciatic nerve was exposed and ligated with 6-0 PGA suture (Akiyama) around ∼1/3 to 1/2 the diameter of the nerve. In sham-operated mice, the nerve was exposed but not ligated.

Real-time PCRs

Total RNA was prepared from L5 DRG using sepasol-RNA I (Nacalai Tesque), chloroform (Sigma-Aldrich), and isopropanol (Sigma-Aldrich), or prepared from ankle joint tissue using a GenElute Mammalian Total RNA Kit (Sigma-Aldrich). The RNA was then treated with DNase I (Sigma-Aldrich) and used for reverse transcription with M-MLV reverse transcriptase (Promega) using an Oligo(dT)18 primer. The cDNA product was used in each real-time PCR reaction. Genomic DNA was prepared from L5 DRG and mouse ankle joints injected with HSV2 using the alcohol precipitation carrier Ethachinmate (Nippon Gene) and isopropanol.

A 7300 Fast Real-Time PCR system and PROBE qPCR Master Mix (KAPA Biosystems) were used to quantify the levels of c-fos

and hypoxanthine phosphoribosyltransferase 1 (HPRT) mRNA and HSV2 DNA.

The TaqMan PCR primer pairs were as follows: mouse HPRT primers, 5′-AGCCCCAAAATGGTTAAGGTTG-3′ and 5′-CAAGGG CATATCCAACAACAAAC-3′; mouse c-fos primers, 5′-CCTTCT CCAGCATGGGCTC-3′ and 5′-CGTGGGGATAAAGTTGGCACTA-3′; and HSV2 primers, 5′-CGCATCAAGACCACCTCCTC-3′ and 5′-GCTCGCACCACGCGA-3′. The TaqMan probes were as follows: mouse HPRT probe, 5′-GATCCAACAAAGTCTGGCCTGTATCCA ACAC-3′ [TAMRA (5-carboxytetramethylrhodamine)]; mouse c-fos probe, 5′-GTGTCAACACAGGACTTTTGCGCAGAT [TAM RA]; and HSV2 probe, 5′-GCGGCGATGCGCCCCAG [TAMRA].

The conditions for TaqMan real-time PCR were 40 cycles at 95°C for 3 s followed by 40 cycles at 60°C for 30 s. The relative mRNA expression levels were normalized to the levels of HPRT mRNA. The relative HSV2 DNA replication levels were normalized to the levels of genomic DNA quantity.

A 7300 Fast Real-Time PCR system (Applied Biosystems) and SYBR green qPCR Master Mix (KAPA Biosystems) were used to quantify the levels of IL-6, CCL2, CCL3, CCL21, CXCL2, and HPRT mRNA.

The PCR primer pairs were as follows: mouse HPRT primers, 5′-GATTAGCGATGATGAACCAGGTT-3′ and 5′-CCTCCCATCTCC TTCATGACA-3′; mouse IL-6 primers, 5′-GAGGATACCACTCCC AACAGACC-3′ and 5′-AAGTGCATCATCGTTGTTCATACA-3′; and mouse CCL2 primers, 5′- CCGGCTGGAGCATCCACGTGT-3′ and 5′- TGGGGTCAGCACAGACCTCTCTCT-3′.

The conditions for real-time PCR were 40 cycles at 94°C for 15 s followed by 40 cycles at 60°C for 60 s. The relative mRNA expression levels were normalized to the levels of HPRT mRNA.

Frozen and paraffin-embedded section preparations and immunohistochemistry

Spines and ankle joints were harvested, and spinal cord segments were separated. Individual spinal cord segments and ankle joints were embedded in a SCEM compound (SECTION-LAB). The cut surface was covered with adhesive film (Cryofilm type IIIC [16UF]; SECTION-LAB), and frozen sections (10–20 µm) were prepared with a cryostat (CM3050S) or a macrotome (CM3600XP; Leica Microsystems) according to a method described previously (Kawamoto and Kawamoto, 2012). For paraffin-embedded sections, ankle joints were harvested, fixed with 10% phosphate-buffered formalin, and embedded in paraffin. The resulting sections were stained with the antibodies described above and counterstained with Hoechst 33342 (Invitrogen), followed by analysis with a BZ-9000 microscope (KEYENCE) or LSM980 (Carl Zeiss).

Quantification of immunostaining

The phosphorylated c-fos+, c-fos+, MHC II+, CD11b+, CD4+, pp65+, and pSTAT3+ areas were measured using ImageJ (Wayne Rasband; National Institutes of Health). Colocalization was measured using the Coloc module of Imaris software (Bitplane).

Electrical stimulation of tibial nerves and recording of electrophysiological signals

C57BL/6 mice were anesthetized with urethane. The core body temperature was maintained at 37.0–37.5°C using a thermostatically regulated heating pad and lamp (ATC-101B-RS; Unique Medical). The tibial nerve around the ankle on the right or left side was stimulated with an electrical square wave pulse of 0.5 ms every 3 s using a stimulator and an isolator (SEN-7203 and SS-202J; Nihon Kohden). The L5 dorsal root, isolated close to the DRG (n = 5), and/or sciatic nerve, isolated at the thigh or around the ankle (n = 5), was placed on bipolar platinum–iridium wire electrodes to detect electrophysiological signals by means of a preamplifier (MEG-6100; Nihon Kohden), an analog-digital converter (Micro 1401; Cambridge Electronic Design), and software (Spike 2; Cambridge Electronic Design). The nerves were covered with warm liquid paraffin. The responses induced by the electrical stimulation were averaged (≥10 trials) using the software.

Spinal cord cut

A skin incision was made along the vertebra at the thoracic to lumbar level, and muscle and vertebral arch were removed. The spinal cord was exposed and cut lengthwise in the center at the T9–13 levels at 0.5–0.6 mm depth with a sharp blade. The mice were not paralyzed. Mice in the sham-operated control group had the muscle and vertebral arch removed, but the spinal cord was kept intact. Experiments using the mice were done 10–14 d after the operation.

Luciferase reporter assay

Ankle joints from NF-κB-reporter Tg/F759 mice were collected, and synovial tissues were homogenized in passive lysis buffer (Promega). After centrifugation, the supernatants were collected, and the total protein amount was adjusted using the Bradford assay. The luciferase activities of tissue lysates were measured using the Luciferase reporter assay system (Promega).

ATP assay

Ankle joints from individual mice were collected and soaked in 10 ml of distilled water containing 10 mM Hepes-NaOH and 250 mM sucrose for 30 min. After 10 min of 3,000 rpm centrifugation at 4°C, the supernatants were collected. The levels of ATP were determined with a luciferin–luciferase assay using an ATP Measuring Reagent Kit (TOYO Ink) according to the manufacturer's instructions, except that the homogenization step was omitted.

ELISA

IL-6 levels in the cell culture supernatant and mouse sera were determined using ELISA kits (BD Biosciences). The levels of norepinephrine, CGRP, bradykinin, and substance P in mouse ankle joints were determined using ELISA kits (LDN; Phoenix Pharmaceuticals; or R&D systems). The level of neuropeptide Y in the mouse ankle joint was determined using ELISA kits (EMD Millipore Corporation). Human IL-6 and mouse IL-17 levels in the sera were determined using ELISA kits (Biolegend and eBioscience, respectively).

Cells and stimulation conditions

The Col1a+ endothelial BC1 cell line was obtained from Dr. M. Miyasaka (Osaka University, Osaka, Japan). W26 synovial

fibroblasts were prepared as described previously (Igarashi et al., 2010). For stimulation, the cells were plated in 96-well plates (1 × 104 cells/well) and stimulated with human IL-6 (50 ng/ml; Toray Industries) plus human soluble IL-6Rα (50 ng/ml; R&D Systems) and mouse IL-17A (50 ng/ml; R&D Systems) for 24 h. The cell culture supernatant was collected for ELISA, and cell growth was assessed by the MTT [3-(4,5-Dimethyl-2-thiazolyl)-2,5-diphenyltetrazolium Bromide] assay (see below).

MTT assay

Cell growth was determined with thiazolyl blue tetrazolium bromide according to the manufacturer's instructions (Sigma-Aldrich).

CIA

CIA was induced in C57BL/6 mice essentially as previously described (Kitabayashi et al., 2010; Sasai et al., 1999). Mice were injected intradermally in their backs with 200 µg of chicken type II collagen (Sigma-Aldrich) plus 250 µg of *Mycobacterium bovis* Bacillus Calmette-Guerin cell wall skeleton (BCG-CWS) emulsified in CFA. 3 wk after the initial injection, a booster injection containing 200 µg of chicken type II collagen plus 250 µg of BCG-CWS emulsified in CFA was given intradermally in the base of the tail. Clinical arthritis activity was evaluated every 2 or 3 d after the second immunization for 21 d. Arthritis severity in the metacarpophalangeal, metatarsophalangeal, and ankle joints was scored using the following scale: 0 = no arthritis, 1 = small degree of arthritis, 2 = mild swelling, 3 = moderate swelling, and 4 = severe swelling. The arthritic score was the sum of the scores from the involved joints in the hind limb.

Statistical analysis

The Student's *t*-test (two-tailed) or Welch's *t*-test was used for the statistical analysis of differences between two groups. Dunnett's test was used for multiple comparisons. The Wilcoxon rank-sum test was used for the statistical analysis of the clinical scores of the arthritis models. Statistical analysis was performed assuming a normal distribution. P values <0.05 are considered statistically significant.

Online supplemental material

Fig. S1 shows the phenotypes of cytokine-induced arthritis and sensory neurons in L5 DRG innervated in the ankle joint. Fig. S2 shows neural activation after cytokine or ATP injection in the ipsilateral joint of F759 mice or WT mice. Fig. S3 shows the increase of CREB activation, ATP synthesis, and clinical score in the contralateral joint by neural activation but not by systemic stimulation of joint-injected cytokines.

Data availability

The datasets generated during and/or analyzed during the current study are available from the corresponding author on reasonable request.

Acknowledgments

The authors thank Dr. G. Karsenty (Baylor College of Medicine, Houston, TX) for the type I collagen-Cre mice, Dr. K. Rajewsky (Harvard Medical School, Boston, MA) for the IKKγflox/flox mice, Dr. Ulrich A.K. Betz (Merck KGaA, Darmstadt, Germany) for the gp130flox/flox mice, and Dr. S. Akira (Osaka University, Osaka, Japan) for the STAT3flox/flox mice. We appreciate the excellent technical assistance and secretarial assistance provided by Ms. N. Kumai, Ms. C. Nakayama, Ms. M. Ezawa, Mr. T. Ohki, and Ms. S. Fukumoto. We thank Dr. P. Karagiannis (Center for iPS Cell Research and Application, Kyoto University, Kyoto, Japan), Dr. K. Tainaka (Niigata University, Niigata, Japan), and Dr. S. Sakoda (Toneyama Hospital, Osaka, Japan) for carefully reading the manuscript and providing many suggestions.

This work was supported by KAKENHI, Q-Leap (JPMXS0120330644), and Japan Agency for Medical Research and Development (D. Kamimura and M. Murakami), Takeda Science Foundation (M. Murakami), Institute for Fermentation Osaka (M. Murakami), Mitsubishi Foundation (M. Murakami), Chugai Pharma Research Grant (M. Murakami), and Akiyama Life Science Foundation (M. Murakami). This study was also supported partly by the Grant for Joint Research Program of the Institute for Genetic Medicine, Hokkaido University, by the Photo-excitonix Project, Hokkaido University, and by the Promotion Project for Young Investigators at Hokkaido University (M. Murakami).

Author contributions: M. Murakami conceived the project and supervised all experiments. M. Murakami and R. Hasebe wrote the manuscript. M. Murakami, R. Hasebe, K. Murakami, N. Halaka, M. Halaka, and Y. Tanaka performed almost all the experiments. The other authors contributed to specific analyses.

Disclosures: The authors declare no competing interests exist.

Submitted: 28 September 2021
Revised: 26 January 2022
Accepted: 16 March 2022

References

Arima, Y., M. Harada, D. Kamimura, J.H. Park, F. Kawano, F.E. Yull, T. Kawamoto, Y. Iwakura, U.A.K. Betz, G. Marquez, et al. 2012. Regional neural activation defines a gateway for autoreactive T cells to cross the blood-brain barrier. *Cell*. 148:447–457. https://doi.org/10.1016/j.cell.2012.01.022

Arima, Y., D. Kamimura, T. Atsumi, M. Harada, T. Kawamoto, N. Nishikawa, A. Stofkova, T. Ohki, K. Higuchi, Y. Morimoto, et al. 2015. A pain-mediated neural signal induces relapse in murine autoimmune encephalomyelitis, a multiple sclerosis model. *Elife*. 4:e08733. https://doi.org/10.7554/eLife.08733

Arima, Y., T. Ohki, N. Nishikawa, K. Higuchi, M. Ota, Y. Tanaka, J. Nio-Kobayashi, M. Elfeky, R. Sakai, Y. Mori, et al. 2017. Brain microinflammation at specific vessels dysregulates organ-homeostasis via the activation of a new neural circuit. *Elife*. 6:e25517. https://doi.org/10.7554/eLife.25517

Arnett, F.C., S.M. Edworthy, D.A. Bloch, D.J. McShane, J.F. Fries, N.S. Cooper, L.A. Healey, S.R. Kaplan, M.H. Liang, and H.S. Luthra. 1988. The American Rheumatism Association 1987 revised criteria for the classification of rheumatoid arthritis. *Arthritis Rheum.* 31:315–324. https://doi.org/10.1002/art.1780310302

Atsumi, T., K. Ishihara, D. Kamimura, H. Ikushima, T. Ohtani, S. Hirota, H. Kobayashi, S.J. Park, Y. Saeki, Y. Kitamura, and T. Hirano. 2002. A point mutation of Tyr-759 in interleukin 6 family cytokine receptor subunit gp130 causes autoimmune arthritis. *J. Exp. Med.* 196:979–990. https://doi.org/10.1084/jem.20020619

Atsumi, T., R. Singh, L. Sabharwal, H. Bando, J. Meng, Y. Arima, M. Yamada, M. Harada, J.J. Jiang, T. Hirano, et al. 2014. Inflammation amplifier, a

new paradigm in cancer biology. *Cancer Res.* 74:8–14. https://doi.org/10.1158/0008-5472.CAN-13-2322

Atsumi, T., H. Suzuki, J.J. Jiang, Y. Okuyama, I. Nakagawa, M. Ota, Y. Tanaka, T. Ohki, K. Katsunuma, K. Nakajima, et al. 2017. Rbm10 regulates inflammation development via alternative splicing of Dnmt3b. *Int. Immunology*. 29:581–591. https://doi.org/10.1093/intimm/dxx067

Burnstock, G. 2006. Historical review: ATP as a neurotransmitter. *Trends Pharmacol. Sci.* 27:166–176. https://doi.org/10.1016/j.tips.2006.01.005

Chavan, S.S., V.A. Pavlov, and K.J. Tracey. 2017. Mechanisms and therapeutic relevance of neuro-immune communication. *Immunity*. 46:927–942. https://doi.org/10.1016/j.immuni.2017.06.008

Chelmicka-Schorr, E., M.N. Kwasniewski, and R.L. Wollmann. 1992. Sympathectomy augments adoptively transferred experimental allergic encephalomyelitis. *J. Neuroimmunol.* 37:99–103. https://doi.org/10.1016/0165-5728(92)90160-m

Clarke, G.S., J.C. Buckland-Wright, and R. Grahame. 1994. Symmetry of radiological features in the wrist and hands of patients with early to moderate rheumatoid arthritis: A quantitative microfocal radiographic study. *Br. J. Rheumatol.* 33:249–254. https://doi.org/10.1093/rheumatology/33.3.249

Donaldson, L.F., D.S. McQueen, and J.R. Seckl. 1995. Neuropeptide gene expression and capsaicin-sensitive primary afferents: Maintenance and spread of adjuvant arthritis in the rat. *J. Physiol.* 486:473–482. https://doi.org/10.1113/jphysiol.1995.sp020826

Fujita, M., Y. Yamamoto, J.J. Jiang, T. Atsumi, Y. Tanaka, T. Ohki, N. Murao, E. Funayama, T. Hayashi, M. Osawa, et al. 2019. NEDD4 is involved in inflammation development during keloid formation. *J. Invest. Dermatol.* 139:333–341. https://doi.org/10.1016/j.jid.2018.07.044

Grassel, S.G. 2014. The role of peripheral nerve fibers and their neurotransmitters in cartilage and bone physiology and pathophysiology. *Arthritis Res. Ther.* 16:485. https://doi.org/10.1186/s13075-014-0485-1

Harada, M., D. Kamimura, Y. Arima, H. Kohsaka, Y. Nakatsuji, M. Nishida, T. Atsumi, J. Meng, H. Bando, R. Singh, et al. 2015. Temporal expression of growth factors triggered by epiregulin regulates inflammation development. *J. Immunol.* 194:1039–1046. https://doi.org/10.4049/jimmunol.1400562

Higuchi, H., D. Kamimura, J.J. Jiang, T. Atsumi, D. Iwami, K. Hotta, H. Harada, Y. Takada, H. Kanno-Okada, K.C. Hatanaka, et al. 2020. Orosomucoid 1 is involved in the development of chronic allograft rejection after kidney transplantation. *Int. Immunol.* 32:335–346. https://doi.org/10.1093/intimm/dxaa003

Hirano, T., and M. Murakami. 2020. COVID-19: A new virus, but a familiar receptor and cytokine release syndrome. *Immunity*. 52:731–733. https://doi.org/10.1016/j.immuni.2020.04.003

Holton, P. 1959. The liberation of adenosine triphosphate on antidromic stimulation of sensory nerves. *J. Physiol.* 145:494–504. https://doi.org/10.1113/jphysiol.1959.sp006157

Igarashi, H., J. Hashimoto, T. Tomita, H. Yoshikawa, and K. Ishihara. 2010. TP53 mutations coincide with the ectopic expression of activation-induced cytidine deaminase in the fibroblast-like synoviocytes derived from a fraction of patients with rheumatoid arthritis. *Clin. Exp. Immunol.* 161:71–80. https://doi.org/10.1111/j.1365-2249.2010.04163.x

Kamimura, D., Y. Tanaka, R. Hasebe, and M. Murakami. 2020. Bidirectional communication between neural and immune systems. *Int. Immunol.* 32:693–701. https://doi.org/10.1093/intimm/dxz083

Kawamoto, T., and K. Kawamoto. 2012. Preparation of thin frozen sections from nonfixed and undecalcified hard tissues using Kawamot's film method (2012). *Methods Mol. Biol.* 1130:149–164. https://doi.org/10.1007/978-1-62703-989-5_11

Kawano, F., A. Ishihara, J.L. Stevens, X.D. Wang, S. Ohshima, M. Horisaka, Y. Maeda, I. Nonaka, and Y. Ohira. 2004. Tension- and afferent input-associated responses of neuromuscular system of rats to hindlimb unloading and/or tenotomy. *Am. J. Physiol. Regul. Integr. Comp. Physiol.* 287:R76–R86. https://doi.org/10.1152/ajpregu.00694.2003

Kawano, F., Y. Matsuoka, Y. Oke, Y. Higo, M. Terada, X.D. Wang, N. Nakai, H. Fukuda, S. Imajoh-Ohmi, and Y. Ohira. 2007. Role(s) of nucleoli and phosphorylation of ribosomal protein S6 and/or HSP27 in the regulation of muscle mass. *Am. J. Physiol. Cell Physiol.* 293:C35–C44. https://doi.org/10.1152/ajpcell.00297.2006

Kelly, S., J.P. Dunham, and L.F. Donaldson. 2007. Sensory nerves have altered function contralateral to a monoarthritis and may contribute to the symmetrical spread of inflammation. *Eur. J. Neurosci.* 26:935–942. https://doi.org/10.1111/j.1460-9568.2007.05737.x

Kidd, B.L., P.I. Mapp, S.J. Gibson, J.M. Polak, F. O'Higgins, J.C. Buckland-Wright, and D.R. Blake. 1989. A neurogenic mechanism for symmetrical arthritis. *Lancet.* 2:1128–1130. https://doi.org/10.1016/s0140-6736(89)91491-8

Kitabayashi, C., T. Fukada, M. Kanamoto, W. Ohashi, S. Hojyo, T. Atsumi, N. Ueda, I. Azuma, H. Hirota, M. Murakami, and T. Hirano. 2010. Zinc suppresses Th17 development via inhibition of STAT3 activation. *Int. Immunol.* 22:375–386. https://doi.org/10.1093/intimm/dxq017

Labasi, J.M., N. Petrushova, C. Donovan, S. McCurdy, P. Lira, M.M. Payette, W. Brissette, J.R. Wicks, L. Audoly, and C.A. Gabel. 2002. Absence of the P2X7 receptor alters leukocyte function and attenuates an inflammatory response. *J. Immunol.* 168:6436–6445. https://doi.org/10.4049/jimmunol.168.12.6436

Larsson, J., A. Ekblom, K. Henriksson, T. Lundeberg, and E. Theodorsson. 1991. Concentration of substance P, neurokinin A, calcitonin gene-related peptide, neuropeptide Y and vasoactive intestinal polypeptide in synovial fluid from knee joints in patients suffering from rheumatoid arthritis. *Scand. J. Rheumatol.* 20:326–335. https://doi.org/10.3109/03009749109096808

Lee, J., T. Nakagiri, D. Kamimura, M. Harada, T. Oto, Y. Susaki, Y. Shintani, M. Inoue, S. Miyoshi, E. Morii, et al. 2013. IL-6 amplifier activation in epithelial regions of bronchi after allogeneic lung transplantation. *Int. Immunol.* 25:319–332. https://doi.org/10.1093/intimm/dxs158

Lefevre, S., A. Knedla, C. Tennie, A. Kampmann, C. Wunrau, R. Dinser, A. Korb, E.M. Schnaker, I.H. Tarner, P.D. Robbins, et al. 2009. Synovial fibroblasts spread rheumatoid arthritis to unaffected joints. *Nat. Med.* 15:1414–1420. https://doi.org/10.1038/nm.2050

Malmberg, A.B., and A.I. Basbaum. 1998. Partial sciatic nerve injury in the mouse as a model of neuropathic pain:behavioral and neuroanatomical correlates. *Pain.* 76:215–222. https://doi.org/10.1016/s0304-3959(98)00045-1

Matsuyama, S., Y. Tanaka, R. Hasebe, S. Hojyo, and M. Murakami. 2021. Gateway reflex and mechanotransduction. *Front. Immunol.* 12:780451. https://doi.org/10.3389/fimmu.2021.780451

Meng, J., J.J. Jiang, T. Atsumi, H. Bando, Y. Okuyama, L. Sabharwal, I. Nakagawa, H. Higuchi, M. Ota, M. Okawara, et al. 2016. Breakpoint cluster region-mediated inflammation is dependent on casein kinase II. *J. Immunol.* 197:3111–3119. https://doi.org/10.4049/jimmunol.1601082

Miller, L.E., J. Grifka, J. Scholmerich, and R.H. Straub. 2002. Norepinephrine from synovial tyrosine hydroxylase positive cells is a strong indicator of synovial inflammation in rheumatoid arthritis. *J. Rheumatol.* 29:427–435

Molleston, M.C., M.L. Thomas, and W.F. Hickey. 1993. Novel major histocompatibility complex expression by microglia and site-specific experimental allergic encephalomyelitis lesions in the rat central nervous system after optic nerve transection. *Adv. Neurol.* 59:337–348

Murakami, M., M. Harada, D. Kamimura, H. Ogura, Y. Okuyama, N. Kumai, A. Okuyama, R. Singh, J.J. Jiang, T. Atsumi, et al. 2013. Disease-association analysis of an inflammation-related feedback loop. *Cell Rep.* 3:946–959. https://doi.org/10.1016/j.celrep.2013.01.028

Murakami, M., D. Kamimura, and T. Hirano. 2019. Pleiotropy and specificity: Insights from the interleukin 6 family of cytokines. *Immunity*. 50:812–831. https://doi.org/10.1016/j.immuni.2019.03.027

Murakami, M., Y. Okuyama, H. Ogura, S. Asano, Y. Arima, M. Tsuruoka, M. Harada, M. Kanamoto, Y. Sawa, Y. Iwakura, et al. 2011. Local microbleeding facilitates IL-6- and IL-17-dependent arthritis in the absence of tissue antigen recognition by activated T cells. *J. Exp. Med.* 208:103–114. https://doi.org/10.1084/jem.20100900

Murase, S., and R.D. McKay. 2014. Neuronal activity-dependent STAT3 localization to nucleus is dependent on Tyr-705 and Ser-727 phosphorylation in rat hippocampal neurons. *Eur. J. Neurosci.* 39:557–565. https://doi.org/10.1111/ejn.12412

Nicolas, C.S., S. Peineau, M. Amici, Z. Csaba, A. Fafouri, C. Javalet, V.J. Collett, L. Hildebrandt, G. Seaton, S.L. Choi, et al. 2012. The Jak/STAT pathway is involved in synaptic plasticity. *Neuron.* 73:374–390. https://doi.org/10.1016/j.neuron.2011.11.024

O'Connor, T.M., J. O'Connell, D.I. O'Brien, T. Goode, C.P. Bredin, and F. Shanahan. 2004. The role of substance P in inflammatory disease. *J. Cell Physiol.* 201:167–180. https://doi.org/10.1002/jcp.20061

Ogura, H., M. Murakami, Y. Okuyama, M. Tsuruoka, C. Kitabayashi, M. Kanamoto, M. Nishihara, Y. Iwakura, and T. Hirano. 2008. Interleukin-17 promotes autoimmunity by triggering a positive-feedback loop via interleukin-6 induction. *Immunity*. 29:628–636. https://doi.org/10.1016/j.immuni.2008.07.018

Okuyama, Y., Y. Tanaka, J.J. Jiang, D. Kamimura, A. Nakamura, M. Ota, T. Ohki, D. Higo, H. Ogura, N. Ishii, et al. 2018. Bmi1 regulates IκBα degradation via association with the SCF complex. *J. Immunol.* 201:2264–2272. https://doi.org/10.4049/jimmunol.1701223

Ota, M., Y. Tanaka, I. Nakagawa, J.J. Jiang, Y. Arima, D. Kamimura, T. Onodera, N. Iwasaki, and M. Murakami. 2020. Role of chondrocytes in the

development of rheumatoid arthritis via transmembrane protein 147-mediated NF-κB activation. *Arthritis Rheumatol.* 72:931–942. https://doi.org/10.1002/art.41182

Pavlov, V.A., and K.J. Tracey. 2017. Neural regulation of immunity: Molecular mechanisms and clinical translation. *Nat. Neurosci.* 20:156–166. https://doi.org/10.1038/nn.4477

Peirs, C., S.P.G. Williams, X. Zhao, C.E. Walsh, J.Y. Gedeon, N.E. Cagle, A.C. Goldring, H. Hioki, Z. Liu, P.S. Marell, and R.P. Seal. 2015. Dorsal horn circuits for persistent mechanical pain. *Neuron*. 87:797–812. https://doi.org/10.1016/j.neuron.2015.07.029

Sadikot, R.T., and T.S. Blackwell. 2008. Bioluminescence: Imaging modality for in vitro and in vivo gene expression. *Methods Mol. Biol.* 477:383–394. https://doi.org/10.1007/978-1-60327-517-0_29

Sasai, M., Y. Saeki, S. Ohshima, K. Nishioka, T. Mima, T. Tanaka, Y. Katada, K. Yoshizaki, M. Suemura, and T. Kishimoto. 1999. Delayed onset and reduced severity of collagen-induced arthritis in interleukin-6-deficient mice. *Arthritis Rheum.* 42:1635–1643. https://doi.org/10.1002/1529-0131(199908)42:8<1635::AID-ANR11>3.0.CO;2-Q

Sawa, S.i., D. Kamimura, G.H. Jin, H. Morikawa, H. Kamon, M. Nishihara, K. Ishihara, M. Murakami, and T. Hirano. 2006. Autoimmune arthritis associated with mutated interleukin (IL)-6 receptor gp130 is driven by STAT3/IL-7-dependent homeostatic proliferation of CD4+ T cells. *J. Exp. Med.* 203:1459–1470. https://doi.org/10.1084/jem.20052187

Schmidt-Supprian, M., W. Bloch, G. Courtois, K. Addicks, A. Israël, K. Rajewsky, and M. Pasparakis. 2000. NEMO/IKK gamma-deficient mice model incontinentia pigmenti. *Mol. Cell*. 5:981–992. https://doi.org/10.1016/s1097-2765(00)80263-4

Seltzer, Z., R. Dubner, and Y. Shir. 1990. A novel behavioral model of neuropathic pain disorders produced in rats by partial sciatic nerve injury. *Pain*. 43:205–218. https://doi.org/10.1016/0304-3959(90)91074-S

Sorkin, L.S., K.A. Eddinger, S.A. Woller, and T.L. Yaksh. 2018. Origins of antidromic activity in sensory afferent fibers and neurogenic inflammation. *Semin. Immunopathol*. 40:237–247. https://doi.org/10.1007/s00281-017-0669-2

Stofkova, A., D. Kamimura, T. Ohki, M. Ota, Y. Arima, and M. Murakami. 2019. Photopic light-mediated down-regulation of local alpha1A-adrenergic signaling protects blood-retina barrier in experimental autoimmune uveoretinitis. *Sci. Rep.* 9:2353. https://doi.org/10.1038/s41598-019-38895-y

Takada, Y., D. Kamimura, J.J. Jiang, H. Higuchi, D. Iwami, K. Hotta, Y. Tanaka, M. Ota, M. Higuchi, S. Nishio, et al. 2020. Increased urinary exosomal SYT17 levels in chronic active antibody-mediated rejection after kidney transplantation via the IL-6 amplifier. *Int. Immunol.* 32:653–662. https://doi.org/10.1093/intimm/dxaa032

Takeda, K., T. Kaisho, N. Yoshida, J. Takeda, T. Kishimoto, and S. Akira. 1998. Stat3 activation is responsible for IL-6-dependent T cell proliferation through preventing apoptosis: Generation and characterization of T cell-specific Stat3-deficient mice. *J. Immunol.* 161:4652–4660

Turner, S.L., and F.J. Jenkins. 1997. The roles of herpes simplex virus in neuroscience. *J. Neurovirol.* 3:110–125. https://doi.org/10.3109/13550289709015801

Xie, Z., J. Dai, A. Yang, and Y. Wu. 2014. A role for bradykinin in the development of anti-collagen antibody-induced arthritis. *Rheumatology (Oxford)*. 53:1301–1306. https://doi.org/10.1093/rheumatology/keu015

JEM

Supplemental material

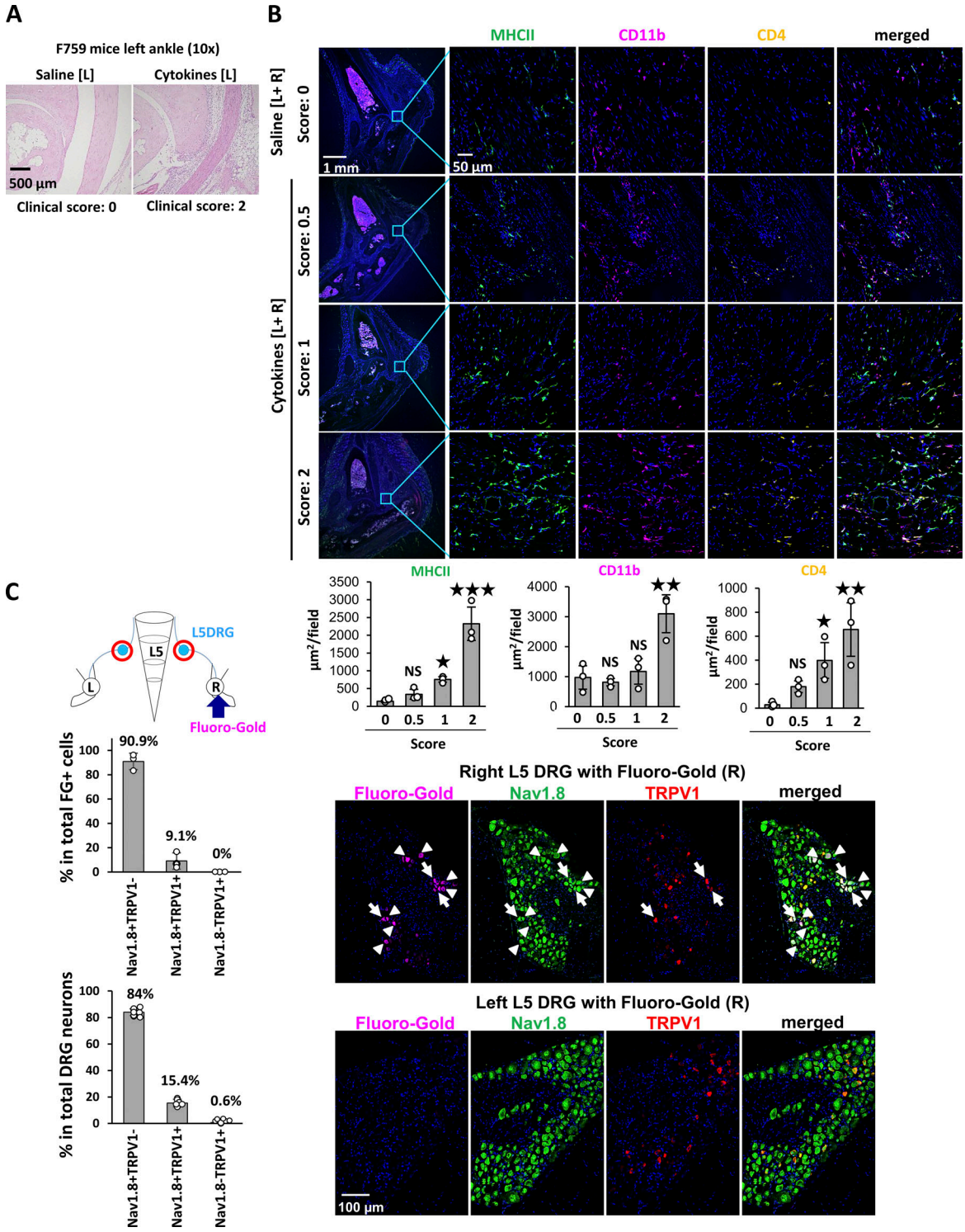

Figure S1. **Phenotypes of cytokine-induced arthritis with activation of sensory neurons in L5 DRG. (A)** Histological analysis of the left ankle joint of F759 mice on day 7 with saline or cytokine injections (IL-17A and IL-6 [0.1 µg each]) on days 0, 1, and 2. Experiments were performed at least three times independently; representative data are shown. **(B)** Immunostaining of MHC II, CD11b, and CD4 in the ankle joints of F759 mice with saline or cytokine injection (IL-17 and IL-6 [0.1 µg each]) bilaterally on days 0, 1, and 2. Experiments were performed three times independently. Bars, 1 mm and 50 µm. MHC II+, CD11b+, and CD4+ areas were quantified from the left or right ankle joints of mice for different clinical scores (n = 3 each). The data are shown as means ± SEM. P values were calculated using Dunnett's test. **(C)** FG was injected into the right ankle joint of F759 mice, followed by the detection of FG and staining of Nav1.8 and TRPV1 in the ipsilateral (right, R) and contralateral (left, L) L5 DRG on day 7. The number of FG+ cells, Nav1.8+TRPV1–, Nav1.8+TRPV1+, and Nav1.8–TRPV1+ cells was counted (n = 3 for the upper graph, n = 6 for the lower graph). The upper graph shows the percentage of FG+ cells in the total number of Nav1.8+TRPV1–, Nav1.8+TRPV1+, and Nav1.8–TRPV1+ cells. The lower graph shows the percentage of Nav1.8+TRPV1–, Nav1.8+TRPV1+, and Nav1.8–TRPV1+ cells in the total number of DRG neurons. Data represent the mean ± SD. Magenta, FG. Green, Nav1.8. Red, TRPV1. Blue, Nuclei. Bar, 100 µm. The diagram illustrates the experimental settings. L, left ankle; R, right ankle. Arrow indicates FG injection, and the red circles indicate the L5 DRGs examined.

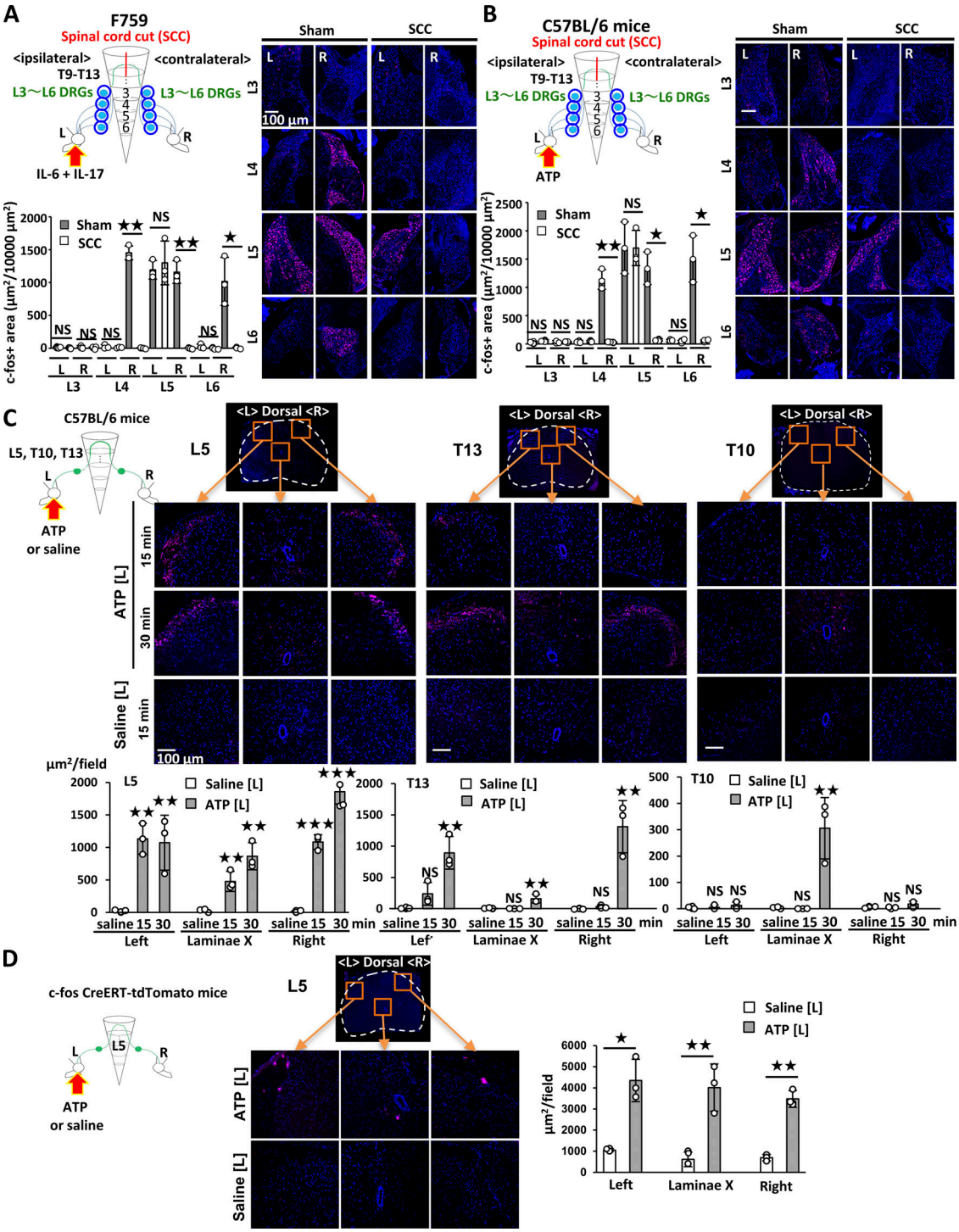

Figure S2. **Neural activation in F759 mice by cytokine injection and WT mice by ATP injection. (A)** c-fos expression of the left (L) and right (R) L3–L6 DRGs in F759 mice who underwent a spinal cord cut (SCC, T9–T13) or sham operation. IL-17A and IL-6 (1 μg each) were injected into the left ankle on days 0, 1, and 2, and c-fos expression was examined by immunostaining on day 3 (n = 3 per group). **(B)** Same as A but ATP (10 μg) was injected into the left ankle on days 0, 1, and 2 (n = 3 per group). For A and B, experiments were performed three times independently. Figures show representative data. c-fos+ areas per 10,000 μm² were quantified (n = 3 each). Mean scores ± SEM were shown. P values were calculated using Student's t-tests or Welch test (*, P < 0.05; **, P < 0.01). Diagrams illustrate the experimental settings. L, left ankle; R, right ankle. Arrows indicate location of the injection. Blue circles indicate the ankle or DRG examined. **(C)** ATP (10 μg) or saline was injected into the left ankle joint of WT mice on day 0, followed by the analysis of phosphorylated c-fos expression in the L5 spinal cord, T13 spinal cord, and T10 spinal cord 15 or 30 min after the last injection. **(D)** ATP (10 μg) or saline was injected into the left ankle joint of c-fos CreERT-Ai14 mice on day 0, 1, 2, followed by the analysis of tdTomato expression in the L5 spinal cord on day 3. For C and D: Magenta, phosphorylated c-fos (C) or tdTomato (D). Blue, nuclei. Bars, 100 μm. Phosphorylated c-fos+ or tdTomato+ areas per field (225,625 μm²) were quantified (n = 3 per group). Experiments were performed three times independently. Mean scores ± SEM are shown. P values were calculated using Dunnett's test (C) or Student's t-test (D; *, P < 0.05; **, P < 0.01; ***, P < 0.001).

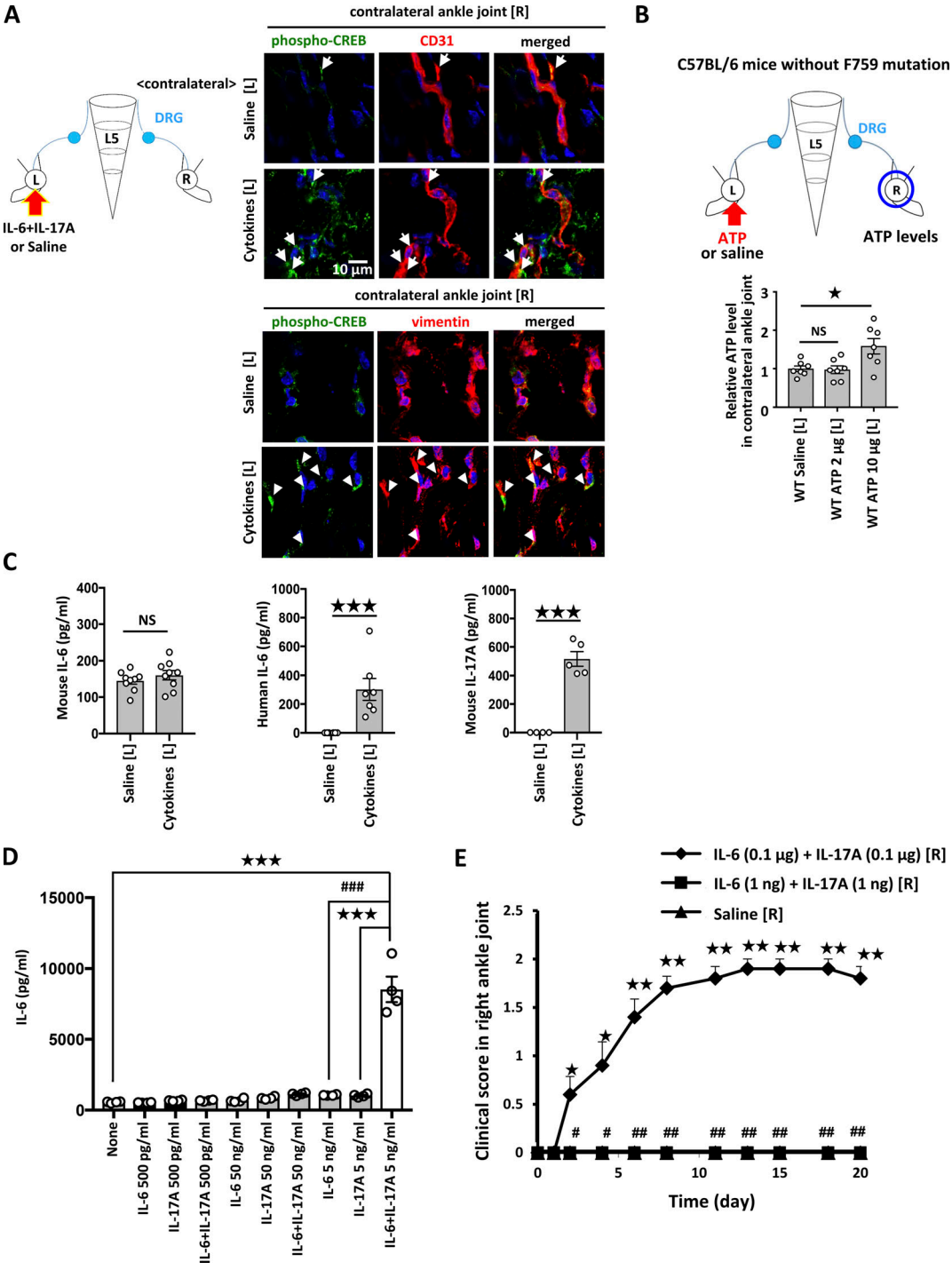

Figure S3. **Neural activation by cytokine or ATP injection induced chemokine expressions and ATP synthesis in the ankle joint on the contralateral sides. (A)** IL-17A and IL-6 (1 μg each) or saline were injected into the left ankle joint of F759 mice on days 0, 1, and 2, followed by immunostaining for pCREB and CD31 or vimentin in the contralateral (right) ankle joint on day 3. Green, phosphorylated-CREB. Red, CD31 or vimentin. Blue, nuclei. Arrows (CD31) and arrowheads (vimentin) show merged signals. **(B)** ATP (2 or 10 μg) or saline was injected into the left ankle joint of naive WT mice on days 0, 1, and 2, followed by the analysis of ATP concentration in the contralateral (right) ankle joint on day 3 (n = 7 per group). For A and B, mean scores ± SEM are shown. P values were calculated using Dunnett's test (*, P < 0.05). The diagrams illustrate the experimental settings. L, left ankle; R, right ankle. Arrows indicate location of the injection. The blue circles indicate the ankle joints examined. **(C)** IL-17A and IL-6 (1 μg each) or saline were injected into the left ankle joint of F759 mice on days 0, 1, and 2, followed by the measurement of mouse IL-6 (n = 9 per group), human IL-6 (n = 6–7 per group), and mouse IL-17A (n = 4–5 per group) levels in serum on day 3. **(D)** BC1 endothelial cells were stimulated with a high (50 ng/ml), medium (5 ng/ml each), or low (500 pg/ml each) dose of IL-6 + IL-17A (human IL-6 plus soluble IL-6Rα and/or mouse IL-17A). Culture supernatants were collected and assessed using an ELISA specific for mouse IL-6 (n = 4 per group). **(E)** IL-17A and IL-6 (0.1 μg or 1 ng each) or saline were injected into the right ankle joint on days 0, 1, and 2. Clinical arthritis scores of the right ankle joint of F759 mice were evaluated (n = 5 per group). Mean scores ± SEM are shown. P values were calculated using Student's t-test (C), Dunnett's test (D), and the Wilcoxon rank-sum test (E; * and #, P < 0.05; ** and ##, P < 0.01; *** and ###, P < 0.001).